# Appendix E

## Characterization of Slurry Phase Iron Catalysts for Fischer-Tropsch synthesis

Linda D. Mansker, Yaming Jin, Dragomir B. Bukur[†], and Abhaya K. Datye[‡]

Center for Micro-Engineered Materials and Chemical and Nuclear Engineering Department
University of New Mexico, Albuquerque, NM 87131-1341, USA

[†] Chemical Engineering Department, MS 3122; Texas A&M University,
College Station, Texas 77843-3122, USA
[‡]To whom all correspondence should be addressed

**ABSTRACT**

The study of Iron Fischer-Tropsch Catalysts by conventional powder X-ray diffraction (XRD) is complicated by the number and type of phases present (α-Fe, various iron carbides, $Fe_xC$: $2 \le x \le 3$, magnetite, $Fe_3O_4$), by peak overlap in the diffraction patterns arising from these phases, and by differences in the ability of each phase to diffract x-rays, which directly influences quantitation. This has led to the consensus that activity for Fischer-Tropsch (F-T) synthesis does not correlate with the bulk composition of the iron catalyst, as seen by x-ray diffraction. As we demonstrate in this paper, some of the problems associated with sample analysis of the working F-T synthesis catalyst originate with the difficulty in preserving the microstructures and composition intact, as the sample is separated from the product and prepared for analysis. Other problems can originate with the way diffraction data are commonly collected and interpreted. In this paper, we present a study of an iron F-T synthesis catalyst, used in a stirred tank reactor, where samples have been removed under inert atmosphere and care was taken to preserve the catalyst constituents intact.

We conducted a systematic, careful analysis of a working Fe-based catalyst, used for two F-T synthesis runs. The reactor was operated under conditions similar to those used for commercial F-T synthesis. Using x-ray diffraction with Rietveld Structure analysis, we demonstrate that we can construct a comprehensive picture of this working catalyst, by correlating the results with the kinetics observed with this catalyst after activation with two different pretreatments, CO and $H_2$. We conclude that, in its most active form, this Fe catalyst contains the so-called ϵ′-carbide (hereafter designated $Fe_7C_3$) and alpha-iron (α-Fe), while the so-called χ-carbide (hereafter designated $Fe_5C_2$), also present in varying amounts during the run, appears to be less active. Our results also show that Soxhlet extraction, a commonly used procedure to remove the wax from a catalyst, can cause changes in catalyst phase composition, and that a separation method based on removal of the wax by warming the sample to reaction temperature and flowing inert gas over it, might present a viable alternative to Soxhlet extraction.

## Introduction

The Fischer-Tropsch (F-T) synthesis, which produces high-molecular weight hydrocarbon wax from syngas, is considered an effective solution to the problem of finding suitable substitutes for liquid fossil fuels. The F-T synthesis reaction converts syngas ($H_2$ / CO, derived from natural gas or coal) to liquid hydrocarbon feed stocks, which can be used for further processing to chemicals, catalytically cracked to various API weight fuels, etc. The choice of catalyst depends upon the syngas ratio ($H_2$ / CO). The $H_2$ / CO ratio is dependent, in turn, upon the syngas precursor and the processing method. A reasonable $H_2$ / CO feed ratio ranges from 1.8 - 2.5, which is typical of natural gas-derived syngas. Coal-derived syngas typically produces an $H_2$ / CO ratio of 0.5-1.7; therefore the catalyst used must possess adequate water gas shift (WGS) activity (in which F-T synthesis product water and CO from the feed are converted to $H_2$ and $CO_2$) to make up the deficit in $H_2$ for the F-T synthesis. Iron F-T synthesis catalysts effectively promote the water-gas shift (WGS) reaction; however, little is known about the iron catalyst composition, morphology or behavior under typical industrial process conditions. Previous attempts to characterize the iron F-T synthesis catalyst have resulted in a great deal of confusion, some of which may arise from the processing thought to be required to obtain a powder sample suitable for analysis, and from subtleties arising from the catalyst phase composition.

Iron F-T synthesis catalysts are prepared by precipitation of a water-soluble iron species (such as $Fe(NO_3)_3$), with or without promoters (such as $KNO_3$ and $Cu(NO_3)_2$) and binders (such as silica). The precipitated powder is then calcined to form hematite ($Fe_2O_3$) and activated by pretreatment with $H_2$, CO, or syngas, outside the reactor or in-situ. Activation alters the catalyst composition to what is thought to be a mixture of iron oxides ($Fe_2O_3$, $Fe_3O_4$), various iron carbides ($Fe_xC$), and iron metal (α-Fe).

There is no agreement over the nature of the working catalyst and the active phase(s) responsible for F-T synthesis. In the literature, we find studies suggesting that magnetite ($Fe_3O_4$) may be the active phase (Butt, 1981; Teichner, 1982), while other workers conclude that the iron carbides ($Fe_xC$) must constitute the active phase(s) (Shroff, et al., 1995, 1996). It is accepted, however, that bulk $Fe_3O_4$ introduced into the F-T synthesis reactor is inactive for the reaction (Huang et al., 1993) and a careful study of catalysts in a fixed bed reactor has clearly linked deactivation of the Fe catalysts to the transformation into $Fe_3O_4$ (Coville et al., 1994).

The fully-reduced iron phase (α-Fe) tends to carbide to the $Fe_5C_2$ phase in syngas; therefore it seems likely that, initially, the $Fe_5C_2$ carbide would be the active phase. However, as shown in this paper, as well as in a companion paper in this special issue (Bukur et al., 1998), a catalyst activated in CO exhibited very low activity initially, despite having almost completely transformed to the $Fe_5C_2$ phase, and exhibited a gradual increase in activity to a high steady state value with time, along with significant compositional changes. This implies that the presence of the $Fe_5C_2$ phase does not guarantee an active catalyst, and some iron phases may be more active than others. However, previous attempts to relate activity to the phase composition have not been successful, and the review paper by Dry (1980) concluded that there is "no reason to relate the amount and nature of iron carbides to F-T synthesis activity."

In order to gain a better understanding of iron F-T synthesis catalyst, we have systematically examined a working catalyst, using x-ray diffraction as the primary analytical technique, taking special care to ensure that the catalyst morphology is preserved during sample preparation and subsequent analysis. The study was performed as a cooperative effort of two laboratories; the catalyst reactivity study was performed at Texas A&M University (TAMU), while the characterization study was performed at the University of New Mexico (UNM). Specifically, we present an analysis of two runs performed in a stirred tank reactor, using identical catalyst precursor. One of the catalysts was activated in CO at 280° C; the other was activated in $H_2$ at 250° C. These runs are part of a larger study of catalyst activation treatments conducted at TAMU, as described elsewhere in this issue (Bukur, et al., 1998).

**Experimental**

The catalyst samples discussed in this paper were obtained from two F-T synthesis runs conducted at Texas A&M University (TAMU). The catalysts were prepared from the same precursor hematite, ($Fe_2O_3$), doped with potassium (K), copper (Cu), and silica ($SiO_2$). The first catalyst was pretreated in $H_2$ at 250°C (run SB-3425, hereafter called the $H_2$-reduced catalyst); the second catalyst was pretreated in CO at 280°C (run SA-0946, hereafter called the CO-reduced catalyst). The details of catalyst preparation, pretreatment, reaction run conditions, and initial experimental behavior for F-T synthesis in a stirred tank reactor are presented elsewhere in this issue (Bukur, et al., 1998).

Characterization studies were performed at TAMU and at the University of New Mexico (UNM) on two sets of slurry samples (catalyst suspended in the waxy product) removed by dip tube under inert atmosphere from the working reactor, at different times during each run, using the method described by Bukur, et al., 1997. The importance of removing F-T synthesis product slurry under inert atmosphere in order to preserve the composition and morphology of the catalyst has been discussed elsewhere (Datye, et al., 1997).

Each slurry sample was split into two portions. One portion of each sample was provided to UNM by TAMU for detailed X-ray and TEM analysis. Diffraction studies of the slurry samples from both runs and of the Soxhlet-extracted powders prepared at TAMU from the $H_2$-reduced run (SB-3425) were performed at UNM. X-ray analysis of Soxhlet-extracted powders from the CO-pretreated run (SA-0946) was performed at TAMU. One slurry sample from the $H_2$-reduced run (SB-3425) was concentrated in our lab by warming the slurry for several days at 150° C under inert atmosphere and letting the catalyst powder concentrate in the bottom portion of the vial. Material was cut from the bottom of the vial and scanned by XRD. The concentrated sample and the remainder of the slurry was then completely stripped of its wax under flowing inert at reaction temperature, for subsequent analysis by x-ray diffraction and high intensity neutron powder diffraction (HIPD), performed at Los Alamos National Laboratory's Manuel Lujan Neutron Science Center (LANSCE).

X-ray diffraction data for slurry and Soxhlet-extracted powder samples from the $H_2$-pretreated catalyst, and for slurry samples from the CO-pretreated catalyst were collected at UNM, using a Scintag PAD-V powder diffractometer with diffracted beam monochromator, operated in step-

scan mode, using Bragg-Brentano (θ-2θ) geometry. Data were collected at 15° to 105°, 0.002° per second for the slurry samples and Soxhlet-extracted powders from the $H_2$-pretreated catalyst (run SB-3425). Data were collected at 10° to 120° 2θ, 0.005° per second for the slurry samples from the CO-pretreated catalyst (run SA-0946). All scans have an average diffraction scan error on the order of ±0 .005° (0.0004 Å). The x-ray diffraction data for the Soxhlet-extracted powders prepared from the samples of CO-pretreated catalyst slurry (run SA-0946) were collected at TAMU, using a Scintag XDS-2000 series powder diffractometer in fast scan (continuous) mode, Bragg-Brentano (θ-2θ) geometry, .0167° per second scan rate, with an average diffraction scan error on the order of ± 0.05° (0.006 Å). In this paper, we will report angles to 2 decimal places, and d-spacings to 3 decimal places.

The UNM diffraction data have been used for phase identification and quantitation, structure analysis, minor phase deconvolution, crystallite size analysis, crystallite shape determination, and evaluation of sample preprocessing methods. None of the diffraction data were subjected to background or polarization correction, or $K_{\alpha 2}$ stripping, prior to analysis and interpretation. Slurries, concentrated slurries, and powders were all pack-mounted in a zero-background substrate sample cell, without any preprocessing, addition of solvent, or grinding. Powders in oil were allowed to settle by gravity, then pack-mounted in the same manner as the slurries. Sample volume required was approximately 0.18cc. Selected samples were periodically re-analyzed at UNM. Multiple data collections on selected samples, carefully preserved, from the $H_2$-pretreated catalyst synthesis run (SB-3425), were performed 24 hours, 1 month, 4 months, 7 months, and 1 year apart, in order to check sample long-term stability, and to validate UNM's analytical procedures. All phase identifications were verified using the diffraction reference data contained in the International Center for Diffraction Data (ICDD), Joint Committee on Powder Diffraction Standards (JCPDS) powder diffraction data base, sets 1 to 46 (ICDD, 1994), and/or from powder diffraction patterns calculated from the single crystal data for the phase (ref. sections I, III).

High Resolution Transmission Electron Microscopy (HRTEM) of samples from runs SB-3425 and SA-0946 was also performed, and the analysis will be discussed in detail elsewhere (Jin and Datye, 1998). We show a few of the micrographs here, to illustrate the effects of Soxhlet extraction on the composition of the working catalyst in run SB-3425. The slurry sample were embedded in epoxy, and thin slices on the order of 40-50 nm were prepared for HRTEM, by ultramicrotomy. The microtomed sections were mounted on a molybdenum grid coated with an holey carbon film, then coated with amorphous carbon to prevent charging. The samples were examined with a JEOL 2010 HRTEM, operated at 200 KeV.

## Results

### I. Calculated Absolute Powder X-ray Diffraction Intensities of Major Iron Phases

As an important step in the characterization of the Iron Fischer-Tropsch catalyst, we will consider in detail how some of the commonly observed phases in the working catalyst appear, by x-ray diffraction,and how they may interfere with one another, when mixed. It is well-known that these materials [e.g., alpha-iron (α-Fe), ϵ′-carbide ($Fe_7C_3$ or $Fe_{2.2}$ C), χ-carbide ($Fe_5C_2$ or $Fe_{2.5}C$), and magnetite ($Fe_3O_4$)] show overlapping diffraction peaks in the region of interest, {25°

$\leq 2\theta \leq 70°\}$. However, most previous analyses, including our own (Shroff, et al., 1995), implicitly assume that the absolute or relative intensities from each phase reflect the relative phase abundances. This is, in fact, not the case.

The powder diffraction database (ICDD, 1994) presents the data for each component in terms of relative diffraction intensities as a function of either $2\theta$ or the d-spacing, in Å. The most intense diffraction peak is set to a value of 100 counts or percent, and all other peakintensities are adjusted accordingly. In principle, the powder diffraction database also lists a **relative intensity ratio** (RIR) factor for each phase, listed as $I/I_{cor}$ on the card, which is the ratio of a given compound's 100% relative intensity peak relative to the 100% relative intensity peak for corundum ( $\alpha$-$Al_2O_3$), in a 50:50 wt % mixture. The $I/I_{cor}$ value is then used to 'correct' the raw 100% peak intensities of each phase for quantitation purposes, by accounting for differences in elemental and compound x-ray scattering cross-section (Bragg, 1949). The $I/I_{cor}$ (or RIR) is used to quantify phases in a mixture, as follows:

$$\frac{w_i}{w_j} = k \frac{I_i}{I_j} \; ; \qquad k = \frac{(I/I_{cor})_j}{(I/I_{cor})_i} \qquad \textbf{(1)}$$

where $W_i$ , $W_j$ , $I_i$ and $I_j$ refer to the weight fractions and diffraction peak intensities for phases i and j, respectively, and k is defined as the $I/I_{cor}$ for phase j divided by the $I/I_{cor}$ for phase i.

The use of $I/I_{cor}$ as an empirical correction factor is based on an assumption that weight percents of the phases in a mixture are similar, and that effects such as preferred orientation, extinction, mixing inhomogeneities, and the breadth of the crystallite size distribution are small enough that the changes in the value of $I/I_{cor}$ are minimal. In the case of the Fischer-Tropsch catalysts, the deviation from equal weight percent mixtures can be substantial; intermediate, disordered, defect or distorted structures are common, particles of material for a given phase can deviate significantly from spherical (preferred orientation or growth habit), and significant anisotropy can occur frequently. The only $I/I_{cor}$ listed in the powder diffraction database is that for hematite ($\alpha$-$Fe_2O_3$, card # 33-664), so we simulated powder diffraction patterns for various iron phase mixtures, in order to estimate $I/I_{cor}$ for the phases not listed, and then experimentally verified those of the oxide phases ($Fe_3O_4$, and $Fe_2O_3$).

We first simulated the diffraction pattern for a 50-50 weight % mixture of $\alpha$-$Al_2O_3$ and the isostructural $\alpha$-$Fe_2O_3$, using single crystal structures from the literature (Thompson, et al., 1987 and Antipin, et al., 1985, respectively), then attempted to reproduce the data experimentally by preparing a 50 wt % calcined hematite and calcined corundum mixture (both from Aldrich Chemical Company, 99.995% purity). The constants describing the instrumental parameters, background function, zero-point error, sample transparency and displacement constants, crystal structure, and crystallite sizes were taken from values obtained determined in our laboratory.

Results were encouraging: we obtained a calculated value of 2.39, and an experimental value of 2.49. These both compare favorable with the value of 2.4 in the literature. This shows that either procedure yields a value that differs from the value of 2.4 listed in the powder diffraction database (ICDD, 1994) by no more than 4.5 %. The results are consistent, thus we are assuming that, for the next set of simulations, the error in experimental and calculated $I/I_{cor}$ will be comparable in magnitude. The details of the simulation and experimental verification method will be published elsewhere (Mansker and Datye, in preparation).

The pattern simulations were performed using the DBWS-9411 Rietveld structure analysis program (Young, 1995, Sakthivel and Young, 1995), following the method of phase quantification of Bish and Howard, 1988 and Hill, 1987, 1993. The Rietveld method was developed by Hugo Rietveld in 1967, for crystal structure determination using neutron powder diffraction data (Rietveld, 1967), but its application to x-ray powder diffraction data has become wide-spread in the last decade. The method provides detailed information on the structure, morphology, and phase abundances in a polycrystalline sample from first principles; using this method, quantifications are possible down to hundreds of ppm levels. It can also be used to determine particle size (average and distributions), crystal habit, particle shape (indirectly), particle surface roughness, stress and strain in the powder, the nature of lattice vacancies and defects.

Figure 1a shows the plot of the simulated diffraction data for the 5-phase mixture (20 wt% each of α-Fe, $Fe_7C_3$, $Fe_5C_2$, $Fe_3O_4$, and α-$Fe_2O_3$) based on single-crystal data from the literature (Wyckoff, 1960; Senczyk, 1993; Herbstein and Snyman, 1963; Sénateur, J.P., 1967; Dirand and Afqir, 1983; Fleet, M.E., 1981, 1982, 1984, and Antipin, et al., 1985). The 100% relative intensity peaks for each phase have been labeled. Not only does the figure demonstrate the degree of diffraction peak overlap that is characteristic of these materials in the region, 25° to 70° 2θ, it also illustrates that, when absolute intensities are compared, a mixture of the five Fe phases thought to appear in the F-T catalyst can produce a diffraction pattern which appears visually to be a mixture of mostly α-Fe and $Fe_3O_4$, with little or no $Fe_7C_3$, $Fe_5C_2$, or $Fe_2O_3$. An $I/I_{cor}$ is estimated for each of the 5 phases, using $I/I_{cor}|_{hem}$:

$$\frac{I_i}{I_{cor}}(calc) = \frac{I_i}{I_{hem}} \frac{I_{hem}}{I_{cor}} |ref; \qquad \textbf{(2)}$$

and the values are listed in Table 1 along with our experimental values of $I/I_{cor}|_{hem}$ and $I/I_{cor}|_{mag}$ determined in this laboratory (Mansker and Datye, in preparation).

For completeness, the powder patterns for each of the phases contributing to the mixture were simulated, and are plotted in figure 1b. Each phase has been normalized to a maximum intensity of 100, so that the details in each diffraction pattern can be seen. Comparison of the estimated $I/I_{cor}$ values and the composite diffraction pattern (figure 1a) demonstrates that large differences in peak intensities can exist, even though the iron phases are combined at equal wt %. Thus it becomes clear that differences in x-ray scattering cross-sections must be considered when

examining mixed the Fe phase catalysts used for F-T synthesis, and that a simple examination of relative peak heights cannot be used to infer the relative amounts of a material present in the working catalyst, without use of the RIR correction factors ($I/I_{cor}$).

We offer a caveat: the powder patterns shown here for the carbides and magnetite are constructed without accounting for phase disorder or significant distortion, disorder, lattice defects, non-spherical particles, or the bimodal particle size distributions often seen in this catalyst, and should be considered ideal. The kind and number of defects and distortions which can be observed are quite systematic in nature, and will be discussed in detail in another set of papers, in preparation.

## II. Influence of Soxhlet Extraction on Catalyst Morphology

X-ray diffraction characterization of the working catalyst samples from the slurry reactor without preprocessing or separation can be problematic, because of interference from the product wax (discussed in section III) and low initial catalyst loading: generally on the order of 10%. Soxhlet extraction is commonly used to concentrate and separate the catalyst from the product wax. Unfortunately, because it employs solvent at its boiling point (on the order of 80°C, Bukur, 1998), Soxhlet extraction may induce undesirable changes in the powder, leading to deceptive results. We examined the $H_2$-pretreated catalyst sample, unreacted powder in oil (run SB-3425, TOS = 000), and compared it to the Soxhlet-extracted powder from the same sample, using x-ray diffraction (XRD) with quantitative Rietveld structure refinement (QRSR). We performed HRTEM on these two samples, to determine what kinds of morphology changes which might occur on the microscale, during or after extraction.

Figure 2 shows a comparison of the diffraction patterns of the pretreated catalyst suspended in oil, and the pretreated sample after Soxhlet extraction. The oil is of sufficiently low molecular weight that its 1st and 2nd order diffraction peaks show up as broad, diffuse humps, and can be neglected as background. The same is true of the silica contained in the sample.

We make the following observations upon visual inspection: the catalyst in oil contains a prominent peak of α-Fe, along with the characteristic broad, amorphous peaks due to the oil, and the asymmetric, broad peaks with sharper apexes characteristic of amorphous silica. The iron phase appears to have a fairly uniform, large crystallite size (symmetric, nearly Gaussian peak shape, and fairly narrow full-width at half maximum - FWHM). The α-Fe peak in the extracted catalyst is broader, which we attribute to the possible presence of $Fe_5C_2$ phase overlapping with the α-Fe peak. We also observe $Fe_3O_4$. The diffraction peaks are very broad at the base, indicating that the $Fe_3O_4$ may show a bimodal particle size distribution. The height of the α-Fe peak relative to the background is lower than seen in the sample in oil, indicating a smaller wt % of α-Fe in this sample. The α-Fe peak also shows considerable asymmetry with a very broad base which could arise from a bimodal crystallite size distribution, as well as additional overlap with the $Fe_5C_2$ phase.

We must conclude that the observed composition and morphology in the extracted sample is probably not representative of the material in the reactor. Neither $Fe_5C_2$ nor $Fe_3O_4$ should have been present, based on the composition observed in the unreacted catalyst in oil.

The low-magnification micrograph of the Soxhlet-extracted powder, from the $H_2$-pretreated catalyst in oil (Figure 3a), shows material with irregularly shaped particles supported on a matrix that contains finer catalyst particles, silica, and some unreduced iron phase. Note the presence of a pronounced surface halo on the particle surfaces, such as that seen on the particles highlighted by arrows in figure 3a. The high-magnification image of one of these haloed particles (figure 3c) clearly shows the thickness of the surface layer (on the order of 5 nm) and the irregular particle shape. The particle's inner core produces lattice fringes of about 2.03Å, which is characteristic of the α-Fe (110) crystal planes. A similar, but thinner, surface oxidation layer was observed by researchers at UNM on carefully passivated samples of α-Fe (Shroff and Datye, 1995).

The micrographs of the pretreated, unreacted catalyst powder in oil (run SB-3425, TOS = 000) are shown in figures 3b and 3d. The overall catalyst microstructure is similar to the extracted catalyst shown in figures 3a and c, but the particles don't show same the thick, pronounced surface halos on their surfaces. The high magnification view of one of the primary particles (figure 3d, examples indicated by arrow in figure 3b) shows a particle of irregular shape, with a much thinner surface halo. Like the Soxhlet-extracted powder, the particle from the unreacted powder in oil also shows lattice fringes of 2.03Å, characteristic of the α-Fe (110) planes.

The samples from the sample at TOS = 000, seemed to indicate that Soxhlet extraction used to separate the catalyst from the product wax induced significant changes in the catalyst, which are detectable by x-ray diffraction and HRTEM, and that both techniques obtain similar information. It wasn't known whether all of the samples subjected to Soxhlet extraction showed the same type of changes. Accordingly, the rest of the samples, slurry and soxhlet-extracted, for both runs, were examined using XRD. The diffraction patterns of the $H_2$-pretreated catalyst, run SB-3425, slurry and Soxhlet-extracted sample sets, are shown in figures 4a and b (5 samples each, as a function of TOS). The slurry and Soxhlet-extracted samples for the CO-activated run, SA-0946, are shown in figures 4c (6 samples) and d (6 samples, Bukur, 1998). We will examine them for evidence that the extraction process may have induced changes.

Visual inspection of the slurry diffraction patterns in figure 4a ($H_2$-pretreated catalyst) reveals that several peaks remain unchanged with time; these correspond to the wax, α-Fe, and what appear to be trace peaks of carbide, almost too small to identify. While the presence of wax peaks obscures the location of some of the $Fe_3O_4$ peaks, the most prominent $Fe_3O_4$ peaks (indicated in Figure 4b) should have been observed if $Fe_3O_4$ were indeed present in the catalyst slurry. Because they are not observed, we conclude that $Fe_3O_4$ is not present in the slurry samples in statistically significant amounts.

The extracted catalyst diffraction patterns (figure 4b, $H_2$-pretreated catalyst) show the presence of significant amounts of $Fe_3O_4$, which is clearly <u>not</u> present in the slurry samples. Note that the α-Fe peak, which appears consistently in the slurry samples, is completely absent in the extracted

samples, except for TOS = 000 hrs. Even in that sample, its intensity is significantly diminished, as shown in figure 2, and discussed earlier.

Having established that the α-Fe seen in the slurry is lost in the Soxhlet-extracted samples, we next examined the α-Fe 100% intensity peak and tail shapes, to ascertain which carbides might be present in the slurry and extracted samples. In the slurry samples, we see evidence of a shoulder on the right of the α-Fe 100% intensity peak, which is indicative of the presence of $Fe_7C_3$ (100% intensity peak at 44.88°), but no evidence of this phase is seen in the extracted samples. However, the diffraction peaks for $Fe_5C_2$ (021) and (112) (~ 43.39° 2θ/100% and ~42.80° 2θ/51%) are seen to be overlapping to form the most prominent peak in all of the extracted samples, which also includes intensity from the $Fe_3O_4$ (004) diffraction peak (~43.15° 2θ).

For completeness, HRTEM was performed on the Soxhlet-extracted sample from end-of-run, $H_2$-pretreated catalyst, TOS=384 (figures 5 a and c)and on a slurry sample near end-of-run, $H_2$-pretreated catalyst, TOS=330 (figures 5 b and d). We may make the comparison of a slurry sample from one TOS to the extracted sample of another TOS, because the activity of the catalyst at TOS =330 and 384 did not differ very much (section V), and the XRD patterns of the slurry samples at those TOS were very similar in appearance and composition (section V).

The Soxhlet-extracted sample ($H_2$-pretreated run, TOS = 384 hrs, figure 5a) contains primary particles of irregular shape covered with a surface halo. Higher magnification views (figure 5c) illustrate that these surface layers exhibit lattice fringes consistent with $Fe_3O_4$. The rough surface layer seems to indicate that oxidation of the particle surface has occurred.

The low-magnification micrograph of the slurry catalyst sample ($H_2$-pretreated run, TOS = 330 hrs) is shown in Figure 5b. The particles exhibit morphology similar to that seen after Soxhlet extraction, and also show layers on the surface. Again, we have often observed that samples removed from a working reactor always show a surface layer (Shroff et al., 1995), and, that while a surface oxide formed at room temperature is often amorphous, beam-induced heating during observation by HRTEM transforms it into crystalline magnetite ($Fe_3O_4$). The high-magnification image of this catalyst (figure 5d), shows that the surface layers observed in the slurry sample remain amorphous, suggesting that the surface layer does not represent a passivating film. The differences between the sample in slurry and after Soxhlet extraction once again indicate that oxidation of the sample occurs either during or after Soxhlet extraction, which is consistent with the diffraction pattern interpretation (section V).

The CO-pretreated catalyst appears to be quite different from the $H_2$-pretreated catalyst, which is evident from figure 4. An examination of the diffraction patterns (figures 4c and 4d) reveals that much less change in composition and microstructure appears to have taken place after Soxhlet extraction. Only the last sample in the series (TOS=563) shows significant visual evidence of oxidation and morphological changes upon Soxhlet extraction. The wax appears to interfere much less with the iron phases in the slurry diffraction patterns (figure 4c), which is consistent with the average molecular weights and average wax composition determined as a function of TOS, in the course of the structure analysis (sections IV, V).

Comparing Figure 4c with Figure 4a, one can see clearly that a small amount of magnetite is present in all of the slurry samples from the CO-pretreated catalyst, run SA-0946, while no magnetite is present in the working catalyst slurry from the $H_2$-pretreated run, SB-3425. The diffraction pattern for the catalyst slurry sample at TOS = 000 (CO-pretreated catalyst) shows that it may consist of $Fe_3O_4$ and $Fe_5C_2$, primarily. As the reaction proceeds, some of the $Fe_5C_2$ in the slurry is transformed to $Fe_7C_3$ (44.88°), the amount of Fe O $_3$d$_4$ops, and some α-Fe is observed in the samples at TOS = {229 and 354} hrs, as indicated in the diffraction pattern over the range, 44° to 45°, where $Fe_5C_2$, $Fe_7C_3$, and α-Fe fall clear of the product wax, but overlap with one another and with $Fe_3O_4$. In all of the slurry samples, the diffraction peak occurring in that region has shoulders on both sides of the maximum, and its multiple apexes are strong evidence of multiple phases.

Examination of the Soxhlet-extracted samples (figure 4d) indicates at first glance that not much change was induced; however, the α-Fe and $Fe_7C_3$ have disappeared from the samples, and the particle sizes and distribution for $Fe_5C_2$ and $Fe_3O_4$ have changed, showing pronounced bimodality. The bimodality in $Fe_3O_4$ indicates that some material with small particle size, has been oxidized

We will examine one more sample, from the $H_2$-pretreated catalyst run (SB-3425, TOS = 233 hrs). Figure 6 shows six diffraction patterns on the same plot. From bottom to top, we show filtered product wax (EW), wax stripped from the slurry by warming it to reaction temperature (260 C) under flowing inert (SW), the slurry (SL) as removed from the reactor, concentrated catalyst slurry (CC; concentrated in the wax by warming the slurry to 150° under inert atmosphere for several days, and sampling the bottom of the vial), catalyst powder obtained from of the slurry by Soxhlet extraction (EP), and the powder residue left after stripping the slurry of wax under flowing inert gas, analyzed by XRD one month after first analysis by neutron diffraction (SP). Most remarkable is the difference between the stripped and the Soxhlet-extracted powders (SP and EP, respectively). The α-Fe peak is completely gone from the Soxhlet-extracted powder(EP), which now contains a broad $Fe_3O_4$ peak. A large $Fe_5C_2$ peak is seen also in the EP (refer to figure 2, extracted), while the SP appears to contain primarily α-Fe, with trace carbide.

We conclude that Soxhlet extraction of the slurry samples is undesirable, because of possible oxidation of the reduced iron phases which could occur either during extraction or upon subsequent exposure to air. Evidence for slow oxidation of the catalyst in the slurry at room temperature, *despite the protective layer of waxy hydrocarbons*, has been observed in the samples used for quality control and stability checks (see section IV), thus we conclude that the possible oxidation phenomena described here could easily and completely transform highly dispersed α-Fe or carbide phases into $Fe_3O_4$. Hence we have focused on the study of catalysts in the wax.

## III. Interference of the Crystalline Wax with Catalyst in the Slurry

It seems apparent that the high molecular weight, straight-chain hydrocarbon product obtained with an high-α catalyst can be quite crystalline and, its diffraction pattern exhibits significant

overlap with the diffraction patterns of the various Fe phases of interest (refer figure 6). We were concerned that catalyst entrained in the wax was producing the diffraction pattern observed, because the two waxes differed in subtle details and in color, neither being clear nor white. In order to determine if entrainment were a problem, the 'catalyst-free' waxes (EW and SW) were examined by AES to determine how much material, if any, remained suspended in them. Consequently, 10 mg each of the extracted wax and inert-stripped wax were digested and analyzed by atomic emission spectroscopy. The extracted wax (EW) showed a total iron content of 80 ppm, and the stripped wax (SW) a total iron content of 207 ppm. Both are well below our detection limit of 350 ppm for XRD, so we concluded that iron entrained in the separated wax does not contribute significantly to the wax diffraction pattern.

The wax diffraction patterns were subsequently analyzed by the Rietveld method, using the low-density polyethylene (LDPE) crystal structure of Hu and Dorsett, 1989. We obtained a very good model for the wax structure, and subsequently used the refined structure parameters, in combination with various iron oxide, metal and carbide single crystal structures, to evaluate the slurry and extracted samples from the two runs. The complete structure analysis results, with quantitation and correlation to reaction kinetics, is discussed in section IV. Because most people who use x-ray diffraction as a tool don't have the theoretical background required to fully exploit the Rietveld structure method, we also explored physical methods of separating the wax from the catalyst, other than Soxhlet-extraction.

The sample of slurry in which the catalyst was concentrated (CC), when compared with the slurry (SL) and inert-stripped powder (SP), indicates that the concentration and stripping methods do a far better job of maintaining catalyst composition and morphology than does Soxhlet extraction. As additional verification, we analyzed the inert-stripped powder, TOS = 233 hrs, three times, over a period of 4 months, in order to determine if the inert-stripped catalyst remained as stable against oxidation. Neither the neutron diffraction nor the seconde set of x-ray results for the stripped powder (SP) will be presented in detail here; they will be discussed in detail in a separate paper on the samples shown in figure 6, and summarized briefly in the next section.

Comparison of the slurry diffraction pattern (SL) to that of the waxes (EW and SW) shows that the wax accounts for many of the diffraction peaks present in the slurry, and thus wax could be easily misidentified as iron phases, as is evident from the diffraction peak positions listed in Table 2. However, regions of 2θ exist, where no wax peaks interfere with iron phase diffraction peaks. Keeping this in mind, we look for additional detail in the region between 52° and 67° 2θ. $Fe_3O_4$ has two moderately intense peaks which occur at 57° and 62.5°. α-Fe has peaks at 44.74° and 64.94°. $Fe_5C_2$ and $Fe_7C_3$ both have 100% relative intensity peaks which overlap with the α-Fe 100% relative intensity peak, in the range 44° - 45°, at 44.175° and 44.882° 2θ, respectively, but are clear of the wax phase. $Fe_5C_2$ has a fairly intense peak at about 50.48° (~ 12 %), and $Fe_7C_3$ at 25.9° (~ 12%), but, again, the relative intensity ratios with α-Fe and magnetite are such that visual inspection for these phases becomes difficult (ref. Section II).

The catalyst crystallite sizes are small enough (≤ 15 nm) and $I/I_{cor}$ that significant overlap and line broadening can occur in the diffraction pattern (cf. sec. I, table 2, figure 2). In spite of this, presence of either of the iron carbides, in the presence of α-Fe, can be detected visually by

examining the α-Fe peak shape. The α-Fe crystallites in the unprocessed slurry produce a nearly Gaussian peak shape. Asymmetries in the α-Fe 100% intensity peak shape, especially in the tail, are indicative of other phases present, where appearance of a shoulder or 'bumpy' tail to the left suggests $Fe_5C_2$, and where the presence of an asymmetry on the right side of the peak indicates $Fe_7C_3$. Using these criteria, we have ascertained that Fe $C_7$ $_3$s present in the slurry, but that in this sample (TOS = 233 hrs, $H_2$-pretreated catalyst), $Fe_5C_2$ is not.

In summary, visual inspection of the catalyst in the slurry indicates only the presence of α-Fe and $Fe_7C_3$ in the slurry. While the α-Fe peaks occur at 2θ values where there is no overlap with the diffraction peaks attributable to the product wax, some of the carbide peaks do overlap with α-Fe, especially with the 100% intensity peak, making it difficult to make a thorough analysis.

## IV. Quantitative Rietveld Refinement, and Precision and Accuracy

In the previous section, we concluded that regions of 2θ exist where the catalyst diffraction pattern shows no overlap with that of the waxy product, but that the data may not be enough to permit a reasonable determination of the presence or absence quantity of some phases. Applying structural methods to the wax and to the icatalyst can permit us make phase composition determinations, which can be used to evaluate the accuracy of our visual interpretation, and provide an opportunity to test the I\Icor values estimated in section I.

Periodically, other samples were re-analyzed to verify the repeatability and accuracy of our analytical technique, and to check sample stability in the slurry. They were from the $H_2$-pretreated catalyst (run SB-3425): slurry, TOS = 384 hrs (analyzed twice, 7 months apart), and the inert-stripped powder, TOS = 233 hrs (). The results will not be shown here, but can be found in the electronic document available through FETC (Mansker, Jin, and Datye, 1996). After 7 months, the α-Fe peaks, present in the first scan of the slurry (TOS = 384) at 44.74° and 64.94° 2θ, are not present in the same sample, 7 months later. In fact, the second scan appeared little different than the wax diffraction patterns shown in figure 7. Upon applying quantitative Rietveld structure refinement to the 7-month repeat diffraction pattern, we determined that the only iron phase still present was a very disordered crystalline magnetite, of small crystallite size (Mansker and Datye, 1998). This seems to indicate that the iron catalyst is so reactive, that it undergoes changes over time, even when suspended in the wax matrix, if not well-protected from air.

The inert-stripped powder, $H_2$-pretreated catalyst (run SB-3425), was examined 3 times in order to test the separation method (section III) and the compositional/morphological stability of the separated material over time. The powder was analyzed once by neutron diffraction at Los Alamos Neutron Science Center, by x-ray diffraction 1 month later (SP, figure 6), then by x-ray diffraction 4 months after the neutron study. Initial examination of the neutron and the one -month x-ray diffraction pattern indicated that, although the major peak seen in the sample can be easily identified as α-Fe, the phase compositions in the sample could be summarized as a mixture of α-Fe, $Fe_7C_3$ (ND and XRD) and trace magnetite (XRD). The data from the second x-ray scan seems to indicate that some subtle changes have taken place in the powder, with time. The intensity of the iron peak had diminished somewhat, and some of the minor phase peaks had

become more prominent. All of the peak widths broadened, indicating some crystallite breakup may have occurred. Structural refinement of the diffraction data for the x-ray repeat pattern also indicated that the sample composition had changed: more of the sample had oxidized, the volume average crystallite sizes had decreased (e.g., the peaks widths had increased), and the $Fe_7C_3$ had completely transformed to the more stable $Fe_5C_2$!

The data appear to indicate that, while stripping away the wax and carefully passivating the powder is more effective at preserving the catalyst morphology and composition than Soxhlet extraction, the catalyst remains highly reactive, and changes over time. We concluded that FTS samples, no matter how well protected, are still reactive, even in the waxy product. This is further proof that samples should be analyzed in a timely manner. Again, detailed discussion of the 4 stripped powder diffraction analyses, along with the rest of the samples shown in figure 6, will be discussed in a separate publication.

## V. Fischer-Tropsch Reaction Results

Reactivity data for the $H_2$-pretreated (SB-3425) and CO-pretreated (SB-3425) catalysts are included here as figure 7 (Bukur, et al., this issue). The plot indicates reactivity as an apparent first order rate constant instead of % conversion, which seems to provide a more accurate picture of the catalyst's intrinsic reactivity. Actual conversions for these runs are shown in the companion paper by Bukur et al., 1998, which were generally high (80%), and are affected by changes in flow rate as well as reaction temperature. Table 3 shows the process parameters during these runs as a function of time and % conversion at selected times on stream. The reaction kinetics for the catalyst activated in CO at 280°C (SA-0946), show a lengthy induction period, in which the activity starts very low, then rises steadily to its steady state value. The run reaches steady state activity near TOS = 113 hrs, where a slurry sample was obtained, and shows stable activity with time, with some fall off in activity towards the end of the run. The catalyst activated in $H_2$ at 250°C (SB-3425), exhibits high activity at the onset of reaction, which begins to fall at longer run times. The CO-pretreated catalyst shows higher steady state activity than that of the $H_2$-pretreated catalyst. In the next section, we will relate these observed variations in catalyst activity with the phase composition and morphology.

## VI. Catalyst Evolution with Time on Stream

We have shown that the catalyst in each run undergoes subtle, but definite phase changes, which correlate with the changes in the activity profiles. We will now describe these changes in detail, based on data obtained from the slurry samples (figures 4a and 4c), then discuss what this tells us about this particular catalyst's active components, over time. We will contrast the behavior of the catalyst after activation in CO to that of the same catalyst activated in $H_2$. Samples from the CO - activated catalyst (SA-0946) were removed from the reactor at TOS = {0, 113, 229, 354, 427, and 563} hrs. Samples from the $H_2$-activated catalyst (SB-3425) were removed from the reactor at TOS = {0, 111, 233, 330, and 384} hrs. The sample compositions were quantified using the Rietveld structure refinement method (Rietveld, 1967), or the estimated $I/I_{cor}$ with the peak intensity, as observed in the diffraction pattern.

Quantitation data from the $H_2$-activated catalyst (SB-3425) and the CO-activated catalyst (SA-0946) are contained in tables 4 and 5, respectively. Two consistency tests were applied to the $H_2$-activated catalyst results. First, weight percents at TOS = 111 hrs were calculated using the estimated $I/I_{cor}$ and the 100% peak heights, and then using the more rigorous Rietveld structure method. The results are in good agreement with one another. The second consistency test involved applying the $I/I_{cor}$ and Rietveld quantitation methods to the data from TOS = 233, slurry and inert-stripped powder (SP). Recall, from sections III and IV, that the stripped powder was first subjected to a neutron diffraction study, scanned by XRD 1 month later (SP), then scanned again 3 months after that. Stripping of the wax improved the signal considerably as can be seen in Fig. 6. The high intensity of scattering from the α-Fe phase, as manifested in the $I/I_{cor}$ values reported in table 1, means that the carbide peak will be difficult to see by x-ray, when the α-Fe is present. In spite of this, the quantitation of the slurry data appears consistent with the quantitation obtained from the inert-stripped powder.

Referring the reader back to figure 7 and the data in tables 4 and 5, we will now discuss the activity curve for the $H_2$-activated catalyst run (SB-3425). Initially, the crystallite size for TOS = 000 hrs, α-Fe, is on the order of 13.5 nm which is in reasonable agreement with the TEM image reported in Fig. 3. Most of the catalyst appears to transform quickly into $Fe_7C_3$ at TOS = 111 hrs. The Rietveld refinement suggests that it is almost completely transformed into the carbide phase. At this stage, the average crystallite sizes for α-Fe are about 37.9 nm, with $Fe_7C_3$ at about 5.5 nm. The catalyst is active until approximately TOS = 160 hrs, when a fairly sharp drop-off occurs. Coincidentally, the space velocity of feed gas was decreased, and the system took time to reach a new steady state. While the phase composition of the catalyst remains the same, we observe an increase in crystallite size for $Fe_7C_3$ (47 nm) and a slight decrease in that for α-Fe (30 nm) in the sample at 233 hours. XRD analysis of the inert-stripped powder from this sample gave comparable crystallite sizes. The data from the sample at TOS=330 hrs. sample indicates that a major change in phase composition has occurred. The catalyst now contains 85.3% $Fe_5C_2$ and 14.3% $Fe_7C_3$, with respective crystallite sizes of 37.9 nm for α-Fe, 5.3 nm for $Fe_7C_3$, and 7.6 nm for $Fe_5C_2$ (see table 4 and figures 11a, 11b). By TOS=384 hrs, the catalyst appears to have transformed almost completely into the $Fe_5C_2$, according to the x-ray data, with phase compositions of ~2.5% $Fe_7C_3$ (4.5 nm particles) and ~97.5% $Fe_5C_2$ (14.8 nm particles), with trace Fe metal (37.2 nm particles).

The average particle sizes listed above compare favorably with the average particle sizes of seen in the TEM images in figure 3a. The slight differences can be explained by two phenomena. First, XRD determines a volume-average particle size and TEM determines an area-average particle size. Second, XRD is sensitive to the size of the crystalline domains while TEM sees the entire particle, implying that if the particles are polycrystalline aggregates, and not single crystals, the XRD estimate of particle size will be smaller than the TEM size. The TEM image does show that many of the particles in Fig. 3a are not single crystals, and high resolution images, such as the one in Fig. 3c, show the lattice planes in the crystal and allow us to identify the individual crystal phase, and average phase composition is more difficult to estimate from TEM, involving high resolution imaging of numerous crystallites and matching the lattice planes with the expected spacings for each phase. Our limited survey of these particles indicated that the majority of them showed lattice fringes of 2.13 Å, which is consistent with the presence of $Fe_5C_2$.

Hence, the TEM of the slurry at TOS =330 hrs. is in good agreement with the phase composition results of the Rietveld structure analysis. The same is true of the sample from TOS = 384 hrs.

The loss of activity in this catalyst appears to be related to the loss of the α-Fe and $Fe_7C_3$ and concurrent the growth of the $Fe_5C_2$ phase, by TOS = 330. This behavior seems consistent with a conclusion that α-Fe and $Fe_7C_3$ are necessary components of an active catalyst, and $Fe_5C_2$ is less active for F-T synthesis. Although not listed in the table, the relative amounts and volume-average molecular weight of wax were monitored in the sample series, as a function of TOS. Keeping in mind that these are **weight** percents, and that the waxy product distribution could have, on average a molecular weight (MW) of at least 2000 g/mole, Rietveld refinement of the slurries, using two LDPE model structures with MW of 2500 and 1500, respectively, with some disorder, gave a total organic weight percent of 99.98%, for all four samples, TOS = {111, 233, 330, and 384} hrs, with a breakdown of about 35 % material at 2500 g/mole, and 65% material at 1500 g/mole.

The composition and crystallite size data for the CO-activated catalyst run (SA-0946) are listed in table 5. The initial slurry sample (TOS = 000 hrs) consists mainly of $Fe_5C_2$, $Fe_7C_3$, and trace $Fe_3O_4$ at wt % of 86.38, 13.41, and 0.22, respectively, giving a carbide ratio ( $Fe_5C_2$ : $Fe_7C_3$ ) of ~6.44, with corresponding volume average crystallite sizes of about 26.9 nm, 13.7 nm, and 19.3 nm respectively. By TOS = 113 hrs, the data show that a major phase transformation has occurred: a portion of the $Fe_5C_2$ carbide has converted to the $Fe_7C_3$ carbide, with wt% of 52.85, 46.17, and 1 for $Fe_5C_2$, $Fe_7C_3$, and $Fe_3O_4$, respectively. The ratio of these carbides is now 1.14:1, with corresponding crystallite sizes of 11.6 nm, 11.4 nm, and 19.3 nm. This coincides with a maximum in the activity versus time curve for this run. After TOS = 113 hrs, the activity shows a very mild drop, then is relatively constant for a time. The activity begins to drop off again after TOS = 427 hrs. Carbide ratios remain around 1:1, until the sample withdrawn at TOS = 427 hrs, where the ratio decreases to .55:1, then increases to 7.17:1 at TOS = 563 hrs. The $Fe_7C_3$ carbide crystallite sizes are fairly constant, with the $Fe_5C_2$ volume average particle size averaging about ⅔ that of the $Fe_7C_3$ carbide, until TOS = 427 hrs, when the $Fe_5C_2$ particle size is now 1.25 times larger than that of the $Fe_7C_3$ carbide (15.3 nm). At end of run, the $Fe_5C_2$ particle size is 2.6 times that of the $Fe_7C_3$ size of 29.5 nm, which is roughly 2 times that observed for this carbide at TOS = 427 hrs. This appears to coincide with a very mild decrease in reactivity. There is only a trace of $Fe_3O_4$ over the course of reaction and of α-Fe in 3 of the samples {229, 354, and 427 hrs TOS}, although both appear to be present in significant amounts from visual inspection of the XRD patterns (x-ray scattering cross-section effects). The $Fe_3O_4$ particle sizes grow steadily over the course of reaction. We interpret the data to indicate that the initial low kinetic activity of the CO-activated catalyst can be attributed to the initial phase composition, and that the 'induction period' observed corresponds to the time required for the transformation of some of the $Fe_5C_2$ carbide into $Fe_7C_3$ carbide, with a corresponding crystallite size decrease in both phases (increasing surface area). The mild deactivation towards the end of the run seems to be caused by an increase in the $Fe_5C_2/Fe_7C_3$ ratio, and an increase in crystallite size for the iron carbide phases (decreasing surface area).

**Summary**

We report a careful, systematic analysis of the diffraction patterns obtained from working Fe-based catalysts used for F-T reaction runs under conditions similar to those used for commercial F-T synthesis. The initial catalyst formulations differ only in the method of activation. We have attempted to quantify the relative amounts and the average crystallite sizes of the iron phases comprising the catalyst a function of time on-stream in the reactor. We have also examined the commonly-used relative intensity ration ($I/I_{cor}$) powder x-ray data quantitation protocol, and compared it to the more rigorous Rietveld structure method (Rietveld, 1967). We discovered that the powder diffraction database (ICDD, 1994) does not report $I/I_{cor}$ values for most of the Fe phases of interest to F-T synthesis, thus we developed a method to predict them, and verified it experimentally for the iron oxides. We discovered that the $I/I_{cor}$ for the various phases vary by as much as 3 orders of magnitude because of differences in x-ray scattering cross-sections for the materials. This implies that a simple visual examination of peak heights in this system can be very deceptive: the α-Fe or the $Fe_3O_4$ peaks will stand out most prominently in an iron F-T synthesis catalyst mixture, while in actuality, the mixture may contain mostly iron carbide phases.

Diffraction studies, used to explore catalyst stability and analytical accuracy and repeatability, indicate that the catalyst is so reactive to oxygen in its reduced state that, unless great care is exercised, the reduced iron species can transform into oxide ($Fe_3O_4$). Hence, one would expect $Fe_3O_4$ to be the predominant phase observed in x-ray data, as seen in many of the previous studies. However, $Fe_3O_4$ is not the major constituent of slurry-phase Fe catalysts: in these runs we found the total $Fe_3O_4$ content to be less than 1 wt% overall, in a properly protected, used catalyst sample activated in CO. The sample activated in $H_2$ showed no $Fe_3O_4$ at all. We have also found that Soxhlet extraction, commonly used to separate the wax from the catalyst, can cause serious composition and morphology transformations in the catalyst, either during extraction, or upon subsequent exposure of the 'clean' material to air. It is also possible that hot solvent may react with the reduced species, particularly with α-Fe, as indicated in the study of the pretreated catalyst sample subjected to Soxhlet extraction from the $H_2$-activated run (SB-3425, TOS = 000). In view of these potential complications, we examined the catalysts suspended in the hydrocarbon wax.

Upon examination, we found that the crystalline hydrocarbon wax typically produced from a high-α catalyst overlaps extensively with the iron catalyst diffraction pattern resulting from a slurry. We approached the wax interference problem by exploring an alternate means of separating the slurry components, and testing the use of rigorous structure methods, to deconvolute the wax diffraction pattern from the catalyst diffraction pattern. We tried heating the catalyst slurry to reaction temperature and flowing an inert gas over the material. This caused most of the wax to entrain and flow out with the gas, leaving behind the catalyst powder. The wax diffraction pattern was eliminated by this process, but there remains the concern that the heat treatment may cause changes in catalyst structure.

The Rietveld structure refinement method was applied quantitatively to the wax-catalyst slurry samples from two F-T synthesis runs which used the same catalyst, one activated under CO and

one activated under $H_2$, and which showed dramatically different activity profiles. The largest source of uncertainty in the Rietveld refinements of the $H_2$-activated catalyst (SB-3425) derived from the degree of crystallinity of the waxy product; the largest source of uncertainty in the Rietveld refinements of the CO-activated catalyst (SA-0946) derive from low catalyst loading (approximately half that used in SB-3425).

The Rietveld method was first tested on 'clean' wax samples before use in analysis of the slurries, for verification, then applied to the slurries in order to determine phase compositions, and volume-average particle sizes for each phase. The CO-reduced catalyst, at TOS = 000 hrs, contains $Fe_5C_2$, with a small amount of $Fe_7C_3$. No graphite is seen by XRD and the TEM images show only a small fraction of the carbide particles to be covered by graphite. This catalyst exhibits a low initial activity, which increases to a steady state value, with a concomitant break up of $Fe_5C_2$ carbide into ***smaller*** crystallites and some transformation into the $Fe_7C_3$ carbide. We speak of this catalyst in terms of a carbide ratio, which we define as the ratio of $Fe_5C_2$ to $Fe_7C_3$ carbide. As long as the carbide ratio and crystallite size remains fairly constant *and* small, the activity appears to remain high. Activity appears to decrease with increasing carbide ratio, and with increased crystallite sizes, corresponding to loss of surface area. The $H_2$-activated catalyst is completely reduced to α-Fe before reaction. We can state conclusively that this working catalyst has no $Fe_3O_4$ in it. Our refinements suggest that once reaction begins, the catalyst contains a $Fe_7C_3$ with a small amount of α-Fe. This sample begins to show significant deactivation which appears to correlate with steady particle growth, and a nearly complete transformation of the $Fe_7C_3$ carbide to the $Fe_5C_2$ carbide.

Based on the results from both runs, we postulate that, although not the most active carbide, that a significant amount of the $Fe_5C_2$ carbide is required in the catalyst to sustain high activity, and that the most active catalyst must contain $Fe_7C_3$ with a small amount of α-Fe. Further work is necessary to understand the driving force for these phase transformations, and the relative contributions from the these phases to overall F-T activity and selectivity. The XRD quantitation needs to be corroborated with TEM, Mossbauer and neutron diffraction to provide an accurate picture of the relative amounts and particle sizes of the different phases present in a Fe F-T synthesis reactor.

This work has also illustrated that ultramicrotomy can be used to prepare thin sections of the working catalyst in wax for analysis by HRTEM. HRTEM data provide some corroboration of the x-ray diffraction results, further detailing the relationship between the microstructure of a working Fe catalyst and its catalytic reactivity. Future work will attempt a correlation of the x-ray diffraction results with Mossbauer and neutron diffraction data, a thorough analysis of the anomalous absorption behavior, and the x-ray, neutron and magnetic scattering behavior of these materials. A detailed HRTEM study of other iron catalyst samples is in progress, and results are presented elsewhere (Jin and Datye, 1998).

## Conclusions

We have drawn several conclusions from this study:

- Fe catalysts separated from the product wax by Soxhlet extraction can exhibit significant changes in composition and/or morphology, hence it is preferable to rely on analyses of the catalyst in the hydrocarbon wax or develop less-severe methods of catalyst-product separation.

- Diffraction methods can be used effectively to analyze the reacted catalyst samples suspended in the waxy product, without further processing, when combined with rigorous crystal structure analysis; however, other methods to deal with the interferences arising from the highly crystalline product wax with the catalyst diffraction pattern need to be developed for the novice x-ray analyst.

- The absolute intensities of the 100% diffraction lines from the various iron phases can vary by over three orders of magnitude. This implies that a purely visual examination of an x-ray diffraction pattern resulting from the catalyst cannot always provide clues to the relative abundance of the various phases present, unless one accounts for differences in the x-ray scattering cross-sections.

- Interpretation of XRD patterns can be conducted successfully using the Rietveld structure refinement method. The accuracy of this method can be influenced by the concentration and dispersion of the catalyst in the wax, and the length of time over which the data are taken; hence the development of alternative means of concentrating the catalyst in the wax seems necessary.

- The catalyst activated in CO has an initial composition of mostly $Fe_3O_4$ and $Fe_5C_2$, while the catalyst activated in $H_2$ has an initial composition of pure α-Fe; however, once F-T synthesis begins, each catalyst readily transforms into a mixture in which significant amounts of $Fe_7C_3$ and small amounts of α-Fe, are present. In both cases, the catalyst appears to lose activity with a conversion of significant amounts of $Fe_7C_3$ into $Fe_5C_2$ and an accompanying growth in crystallite size.

- We suggest that $Fe_7C_3$ in combination with α-Fe is associated with the most active catalysts. The behavior of the $H_2$-activated catalyst, when compared to that of the CO-activated catalyst, seems also to indicate that the $Fe_5C_2$ carbide, though less active, must be present in the mixture in significant amounts, in order for high activity to be sustained.

## Acknowledgments

This work was supported under the U.S. Department of Energy University Coal Research Grant DE-FG22-95PC95210, with partial support from NSF HRD 93-53208 at the University of New Mexico, and by U. S. Department of Energy Contract DE-AC22-94PC93069 at Texas A&M University. We further acknowledge the X-ray Powder Diffraction Laboratory, Department of

Earth and Planetary Sciences, University of New Mexico, and Los Alamos National Laboratory, Manuel Lujan Neutron Scattering Center.

**References**


Amelse, J.A.; Schwartz, L.H.; and Butt, J.B.; Journal of Catalysis; **72,** 1981, 95.

Antipin, M.I.; Tairelson, V.G.; Flugge, M.P.; Gerr, R.G.; Struchkov, Iu. T.; and Oserov, R.P.; Doklady Akadameii Nauk SSSR; **281**(4), 1985, 854.

Baltrus, J.P; Diehl, J.R.; McDonald, M.A.; and Zarochak, M.F.; Applied Catalysis; **48,** 1989, 199.

Bish, D.L. and Howard, S.A.; Journal of Applied Crystallography, **21,** 1988, 86-91.

Blanchard, F.B.; Raymond, J.P.; Pommier, B.; and Teichner, S.J.; Journal of Molecular Catalysis; **17**, 171 (1982).

Bragg, W.L. and Bragg, W.H., *The Crystalline State: a General Survey*, The Crystalline State, Vol. 1, Bragg, W.L., editor, G. Bell and Sons, ltd., London (1949).

Bukur, D.B.; Nowicki, L.; and Lang, X.; Catalysis Today; **24,** 1995, 111.

Bukur, D.B.; Lang, X.; and Ding, Y.; Preprints of the American Chemical Society Division of Fuels Chemistry; **42**(2), 1997, 623.

Bukur, D.B; Lang, X.; and Ding, Y.; Applied Catalysis, Journal of Applied Catalysis, this issue 1998.

Dictor R.A.and Bell, A.T.; Journal of Catalysis; **97**, 1986, 121.

Dirand, M. and Afqir, L.; Acta Metallurgica; **31**(7), 1983, 1089.

Dorsett, D.L. and Moss, B.; Polymer, **24**(3), 1983, 291.

Dorsett, D.L.; Acta Crystallographica, **B51**, 1995, 1021.

Dorsett, D.L.; Polymer, **27**(9), 1986, 1349.

Dorsett, D.L.; Polymer, **38**(2), 1997, 247.

Dry, M.E.; 'Catalysis - Science and Technology'; J.R. Anderson and M. Boudart, Eds.; Chapter 15, 1980, 160.

Duvenhage, D.J.; Espinoza, R.L.; and Coville, N.J.; Studies in Surface Science and Catalysis; **88,** 1994, 351.

Dwyer, D.J. and Somorjai, G.A.; Journal of Catalysis; **52,** 1978, 291.

Fleet; M.E.; Acta Crystallographica, **B37,** 1981, 917.

Fleet, M.E.; Acta Crystallographica, **B38,** 1982, 1718.

Fleet, M.E.; Acta Crystallographica, **C40,** 1984, 1491.

Fleet, M.E.; Journal of Solid State Chemistry, **62**, 1986, 75.

Herbstein F.H. and Snyman, J.A.; Inorganic Chemistry, **3**(6), 1964, 894.

Hill, R.J.; and Howard, C.J.; Journal of Applied Crystallography, **20,** 1987, 467-474.

Hill, R.J., in the 'The Rietveld Method'; Young, R.A., ed.; International Union of Crystallography, Oxford University Press, Pub.; 1993, 61-101.

Hu, H.L. and Dorset, D.L.; Acta Crystallographica; **B45,** 1989, 283.

Huang, C.S.; Xu, L.; Davis, B.H.; Fuel Science and Technology, International. **11**; 639 (1993).

International Center for Diffraction Data (ICDD), Joint Committee on Powder Diffraction Standards (JCPDS) powder diffraction data base, sets 1-42, 1994.

Jager, B and Espinoza, R.L.; Catalysis Today; **23,** 1995, 17.

Jackson, N. B., Mansker, L. D., O'Brien, R. J., Davis, B. H. and Datye, A. K., Studies in Surface Science and Catalysis, **111,** 1997, 501.
Jin, Y. and Datye, A. K., Proceedings of the International Congress on Electron Microscopy; Cancun 1998, Inst. Of Physics Publishing, **II**, 1998, 379.
Jin, Y. and Datye, A. K., "Characterization of Bubble Column Slurry Phase Iron Fischer Tropsch Catalysts, Natural Gas Conversion V, Stud. Surf. Sci. Catal., vol 119, page 209, 1998.
Kalakkad, D.S.; Shroff, M.D.; Köhler, S.D.; Jackson, N.B.; and Datye, A.K.; Applied Catalysis A; **133,** 1995, 335.
Larson, A.C. and Von Dreele, R.B.; "GSAS: General Structure Analysis Program"; Los Alamos National Laboratory, Los Alamos, NM 87545; 1997.
Mansker, L.D., Jin, Y.; and Datye, A. K.; Proc. Coal Liquefaction and Solid Fuels '97 Conference proceedings, electronic publication, Federal Energies and Technologies Center (FETC), Pittsburgh, Pennsylvania; http://www.fetc.doe.gov/events/97conferences/coal_liq/97cl_pdf/datye.pdf/; 1997.
Mansker, L.D. and Datye, A.K.; in preparation, 1998.
McCartney, J.T.; Hofer, L.J.E.; Seligman, B.; Lecky, J.A.; Peebles, W.C.; and Anderson, R.B.; Industrial and Engineering Chemistry; **57,** 1953, 730.
Moss, B. and Dorsett, D.L.; Acta Crystallographica, **A40**, C318 (1984).
Niemantsverdriet, J.W.; van der Kraan, A.M.; van Dijk, W.L.; and van der Baan, H.S.; Journal of Physical Chemistry; **84**(25), 1980, 3363.
Niemantsverdriet, J.W.; and van der Kraan, A.M.; Journal of Catalysis; **72,** 1981, 375.
O'Brien, R.J.; Xu, L.; Spicer. R.L.; Bao, S.Q.; Milburn, D.R.; and Davis, B.H.; Catalysis Today; **36**(3), 1997, 325.
Okudera, H.,; Kihara, K.; and Matsumoto, T.; Acta Crystallographica, **B52**, 1996, 450.
Rath, L.K. and Longanbach, J.R.; Energy Sources; **13,** 1991, 443.
Raupp, G.B. and Delgass, W.N.; Journal of Catalysis **58,** 1979, 348.
Rao, V.U.S.; Stiegel, G.J.; Cinquegrane, G.J.; and Srivastava, R.D.; Fuel Processing Technology; **30,** 1992, 83.
Rao, K.R.P.M.; Huggins, F.E.; Huffman, G.P.; Gormley, R.J.; O'Brien, R.J.; Davis, B.H.; Energy and Fuels; **10**(3), 1996, 546.
Rietveld, H.M., Acta Crystallographica, **22**, 151 (1967).
Rietveld, H.M., Journal of Applied Crystallography, **2**, 1969, 65.
Sakthivel, A. and Young R.A.; Rietveld Analysis Program DBWS-9411, Release 30.03.95, software, 1995.
Sénateur, J.P.; Annales de Chimie, **2** 1967, 103.
Senczyk, D.; Phase Transitions, **43** 1993, 153.
Shroff, M.D.; Kalakkad, D.S.; Coulter, K.E.; Kohler, S.D.; Harrington, M.S.; Jackson, N.B.; Sault, A. G.; and Datye, A.K.; Journal of Catalysis, **156**(2), 1995, 185-207.
Shroff, M.D.; Datye, A.K; Catalysis Letters, **37**(1-2), 1996, 101-106
Thompson, P; Cox, D.E.; and Hastings, J.B.; Journal of Applied Crystallography, **20,** 1987, 79.
Withers, R.L. and Bursill, L.A., Journal of Applied Crystallography, **13**, 1980, 346.
Wyckoff, R.W.G; New York, 3rd Ed.; Interscience Publishers, 1960.

Young, R.A., ed.; 'The Rietveld Method'; International Union of Crystallography, Oxford University Press, Pub.; 1993.
Young R.A.; Journal of Applied Crystallography, **28,** 1995, 366-367.

**Figure Captions**

Figure 1 a: Simulated X-ray diffraction pattern for a 20 wt% mixture of each of these phases: $Fe_2O_3$, $Fe_3O_4$, α-Fe, $Fe_7C_3$, and $Fe_5C_2$ ;

b: simulated pattern for each phase plotted at full scale: b) $Fe_2O_3$, $Fe_3O_4$, α-Fe, $Fe_7C_3$, and $Fe_5C_2$.

Figure 2: X-ray diffraction pattern from $H_2$-activated run SB-3425, TOS = 000 hrs. Lower curve, sample in the oil, and upper curve: powder after Soxhlet extraction .

Figure 3 a: Low magnification view of catalyst from the $H_2$-activated run SB-3425, TOS = 000 hrs, extracted powder

b: Low magnification view of $H_2$-activated run SB-3425, TOS = 000 hrs, slurry

c: High magnification view of catalyst from the $H_2$-activated run SB-3425, TOS = 000 hrs, extracted powder

d: High magnification view of catalyst from the $H_2$-activated run SB-3425, TOS = 000 hrs, slurry.

Figure 4 a: X-ray diffraction patterns of samples from catalyst from the $H_2$-activated run SB-3425, slurry samples.

b: X-ray diffraction patterns of catalyst from the $H_2$-activated run SB-3425, extracted samples.

c: X-ray diffraction patterns of catalyst from CO-activated run SA-0946, slurry samples.

d: X-ray diffraction patterns of catalyst from CO-activated run SA-0946, extracted samples. Note the loss of preferred orientation in the $Fe_5C_2$ phase, with increasing TOS (*except* in TOS = 563) - this indicates that the particles of a given phase are either breaking up or renucleating. The samples show significant zero-point error, as an S-shaped displacement in the peaks, with TOS. This probably arises from sample prep error, and could not be corrected for directly by UNM, due to lack of access to the raw data. Thus, labeling has been based on the reference angles and/or easily recognizable peak-group shapes.

Figure 5 a: Low magnification view of catalyst, $H_2$-activated run SB-3425, TOS = 384 hrs, extracted powder

b: Low magnification view of catalyst, $H_2$-activated run SB-3425, TOS = 330 hrs, slurry

c: High magnification view of catalyst, $H_2$-activated run SB-3425, TOS = 384 hrs, extracted powder

d: High magnification view of catalyst, $H_2$-activated run SB-3425, TOS = 330 hrs, slurry. Note that figure 5c shows images of the powder, without embedding in epoxy and ultramicrotomy.

Figure 6 X-ray diffraction pattern of catalyst components, $H_2$-activated run SB-3425, TOS = 233 hrs. Original slurry (SL), filtered wax (EW), inert-stripped wax (SW), concentrated catalyst slurry (CC), catalyst after Soxhlet extraction (EP), and catalyst powder obtained after the wax was stripped off in flowing inert (SP). The α-Fe peak seen in the slurry sample grows in size as the catalyst is concentrated,

while the wax peaks diminish in intensity. Note the remarkable difference between the Soxhlet extracted powder and the inert-stripped powder.

Figure 7: Fischer-Tropsch reactivity curves for $H_2$-activated run SB-3425, and CO-actived run SA-0946. The results are plotted in the form of a pseudo-first-order rate constant, referenced to 250°C. The rate constant units are in mmol of CO converted per g Fe per MPa pressure per hour. The reactor was operated at temperatures ranging from 260°C to 266°C and varying space velocities. The process conditions and actual conversion at several times on stream are shown in Table 3.

| Table 1: $I/I_{cor}$ for iron phase mixture (based on $d_p^{avg}$ = 15 nm for all phases) | | | |
|---|---|---|---|
| **Phase** | **$I_{max}$** | **$I\backslash I_{cor}$** | **$I\backslash I_{(Fe5C2)}$** |
| Fe | 5750 | 1526 ± 32 | 4299 |
| $Fe_7C_3$ | 12.19 | 3.237 ±.066 | 9 |
| $Fe_5C_2$ | 1.34 | 0.355 ± .008 | 1 |
| $Fe_3O_4$ | 532.2 | 141.3 ± 3 (c) / 147 (e) | 398 |
| $Fe_2O_3$ | 9.191 | 2.39 (c) ± .049 /2.49 (e) | 6.7 |
| (c) - calculated<br>(e) - experimental, UNM | | | |

| Table 2: d-spacings, angles, and relative intensities in the Wax XRD | | | | | | | |
|---|---|---|---|---|---|---|---|
| **d-spacing, Å** | 2.986 | 2.569 | 2.545 | 2.485 | 2.108 | 1.613 | 1.444 |
| **2θ Angle, °** | 29.9 | 34.9 | 35.24 | 36.12 | 42.86 | 57.04 | 64.46 |
| **% Intensity, extracted** | 79.96 | 45.76 | 48.79 | 100 | 98.39 | 30.18 | 24.74 |
| **% Intensity, stripped** | 62.58 | 42.31 | 42.99 | 66.87 | 100 | 25.84 | 19.11 |

| TABLE 3: Process Changes with corresponding % Conversion | | |
|---|---|---|
| **TOS, hrs** | **SA-0946: Change** | **% conversion** |
| **0** | Sample; T = 260°C; P = 200 PSIG; $H_2$/CO = 0.67; SV = 2.34 Nl/g-cat/h | 36.1 (2h) |
| **113** | Sample | 76.6 (112h) |
| **133** | SV=1.8 Nl/g-cat/h | 76.0 (131h) |
| **229** | Sample | 80.2 (228h) |
| **231** | P = 300 PSIG; SV = 2.64 Nl/g-cat/h | 76.4 (235h) |
| **354** | Sample | 81.1 (351h) |
| **427** | Sample | 81.0 (426h) |
| **443** | $H_2$/CO = 0.6; SV = 2.0 Nl/g-cat/h | 81.5 (442h) |
| **563** | Sample | 81.9 (561) |
| **TOS, hrs** | **SB-3425: Change** | **% Conversion** |
| **0** | Sample; $H_2$/CO = 0.67; T = 260°C; SV = 2.34 Nl/g-cat/h; P = 200 PSIG | 75.8 (1.5h) |
| **111** | Sample | 70.8 (110h) |
| **159** | SV = 1.80 Nl/g-cat/h | 70.2 (157h) |
| **233** | Sample | 73.5 (230h) |
| **278.5** | Power out | 71.8 (276h) |
| **279** | T = 200°C | --- |
| **282** | T = 260°C | 70.0 (287h) |
| **311** | H2/CO = 0.6 | 69.8 (310h) |
| **330** | Sample | 65.1 (329h) |
| **330** | SV = 1.0 Nl/g-cat/h | 81.7 (340h) |
| **355** | T = 266°C | 80.0 (353h) |
| **384** | Sample | 80.1 (383h) |

| Table 4: Estimated wt % of iron phases in SB-3425, Slurry samples | | | | |
|---|---|---|---|---|
| **TOS, hrs** | **α-Fe** | **$Fe_7C_3$ (so-called ϵ′)** | **$Fe_5C_2$ (so-called χ)** | **$Fe_3O_4$** |
| **0** | 100 | 0 | 0 | 0 |
| **111** | 0.02 (QRSR)<br>0.03 ($I/I_{cor}$) | 99.98 (QRSR)<br>98.25 ($I/I_{cor}$) | 0 | 0 |
| **233** | 3.09 | 96.91 | 0 | 0 |
| ***233 (SP1)*** | *1.76* | *89.50* | --- | *8.74* |
| **330** | 0.42 | 14.32 | 85.26 | 0 |
| **384** | .004 | 2.47 | 97.52 | 0 |
| **SB-3425, Slurry samples: Particle sizes, nm** | | | | |
| **TOS, hrs** | **α-Fe** | **$Fe_7C_3$ (so-called ϵ′)** | **$Fe_5C_2$ (so-called χ)** | **$Fe_3O_4$** |
| **0** | 13.54 | | --- | --- |
| **111** | 37.88 | 5.27 | --- | --- |
| **233** | 30.50 | 47.12 | --- | --- |
| **233 (SP1)** | 17.54 | 23.32 | --- | 33.42 |
| **330** | 37.88 | 5.27 | 7.63 | --- |
| **384** | 37.22 | 4.49 | 14.78 | --- |

| Table 5: Estimated wt % of iron phases in SA-0946, slurry samples | | | | |
|---|---|---|---|---|
| **TOS, hrs** | **α-Fe** | **$Fe_7C_3$ (so-called ϵ′)** | **$Fe_5C_2$ (so-called χ)** | **$Fe_3O_4$** |
| **0** | 0.00 | 13.41 | 86.38 | 0.22 |
| **113** | 0.00 | 46.17 | 52.85 | 0.99 |
| **229** | 0.01 | 49.46 | 49.48 | 1.05 |
| **354** | 0.01 | 53.05 | 46.66 | 0.28 |
| **427** | 0.02 | 64.61 | 35.37 | 0.01 |
| **563** | 0.00 | 12.19 | 87.40 | 0.41 |
| **SA-0946, slurry samples: Particle sizes, nm** | | | | |
| **TOS, hrs** | **α-Fe** | **$Fe_7C_3$ (so-called ϵ′)** | **$Fe_5C_2$ (so-called χ)** | **$Fe_3O_4$** |
| **0** | --- | 13.67 | 26.92 | 19.27 |
| **113** | --- | 11.38 | 11.58 | 48.195 |
| **229** | 52.12 | 11.27 | 7.67 | 44.16 |
| **354** | 19.1 | 13.02 | 7.54 | 142.1 |
| **427** | 56.77 | 15.28 | 19.12 | 145.86 |
| **563** | --- | 29.49 | 77.34 | 158.19 |

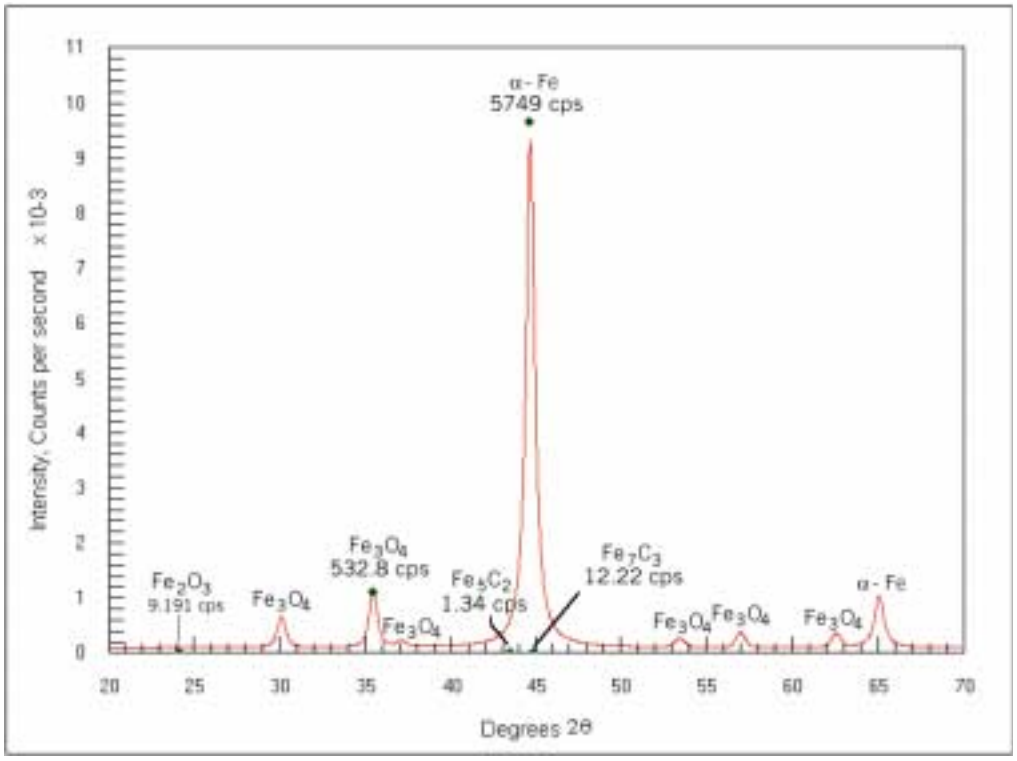


**Figure 1a**

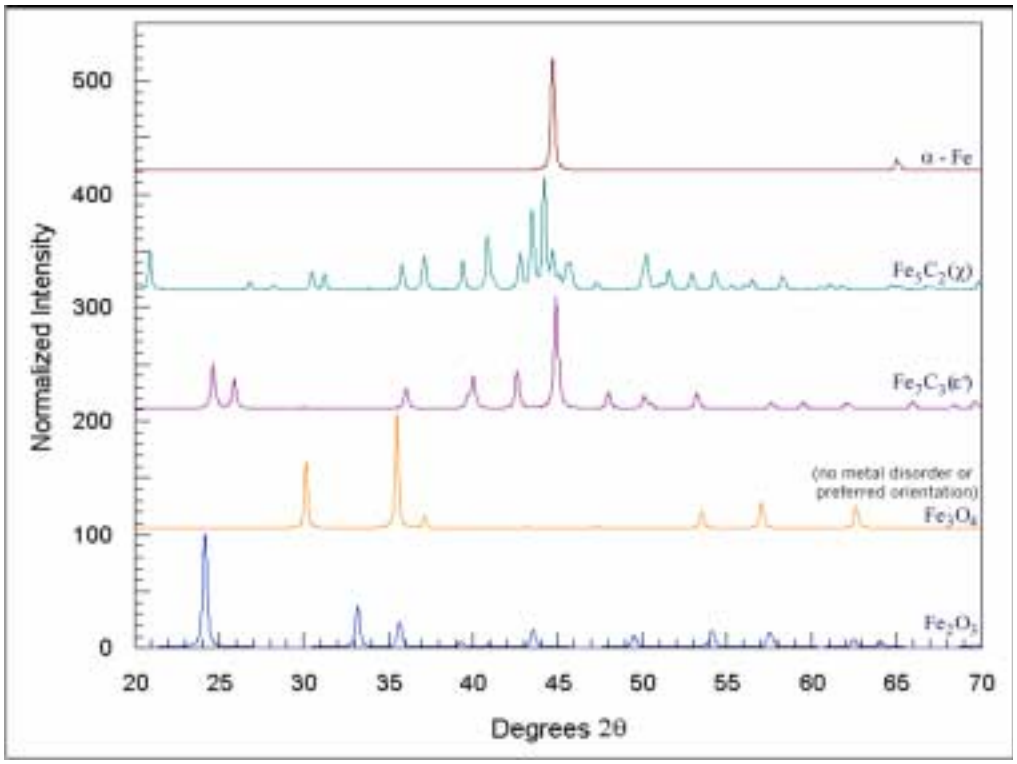


**Figure 1b**

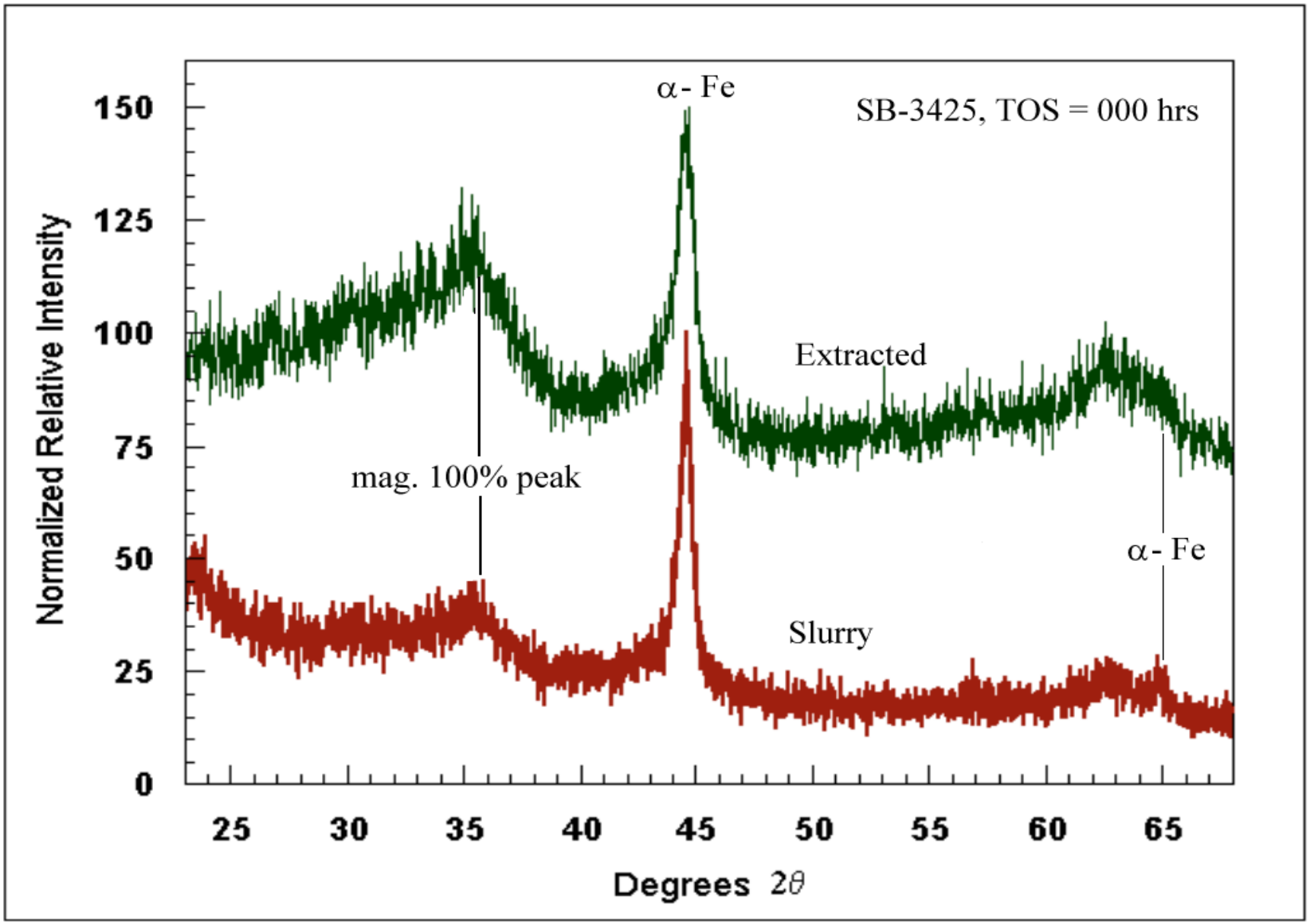
α - Fe
SB-3425, TOS = 000 hrs
Extracted
mag. 100% peak
α - Fe
Slurry
Normalized Relative Intensity
150
125
100
75
50
25
0
25
30
35
40
45
50
55
60
65
Degrees 2θ

**Figure 2**

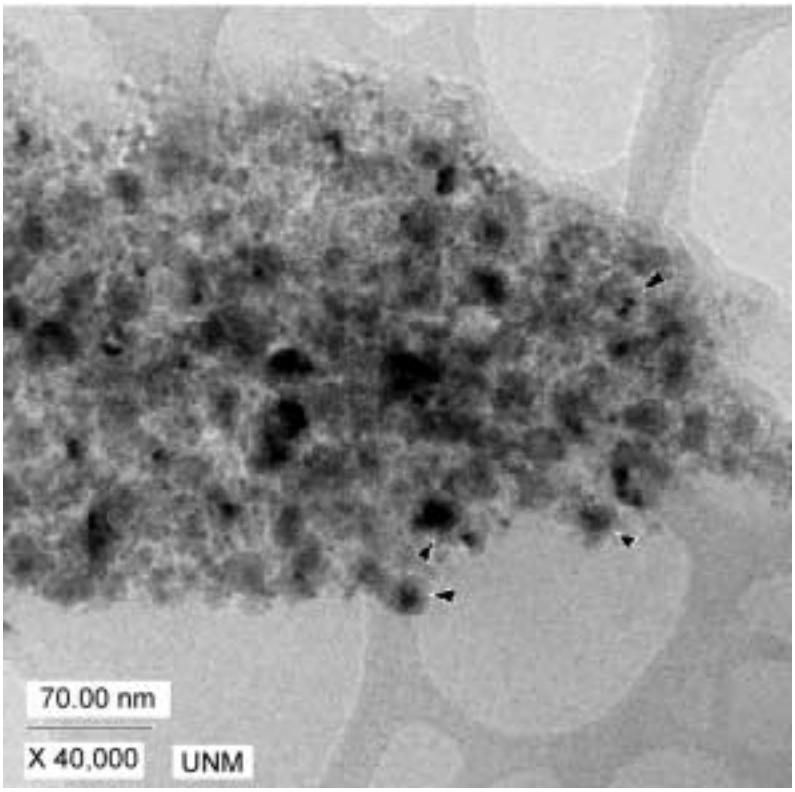


**Figure 3a**

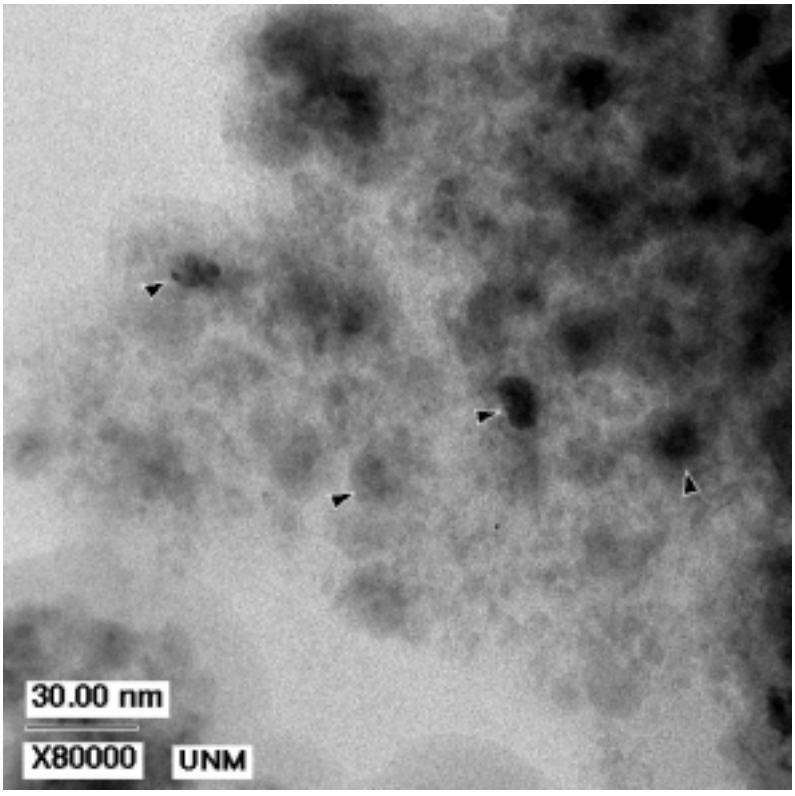


**Figure 3b**

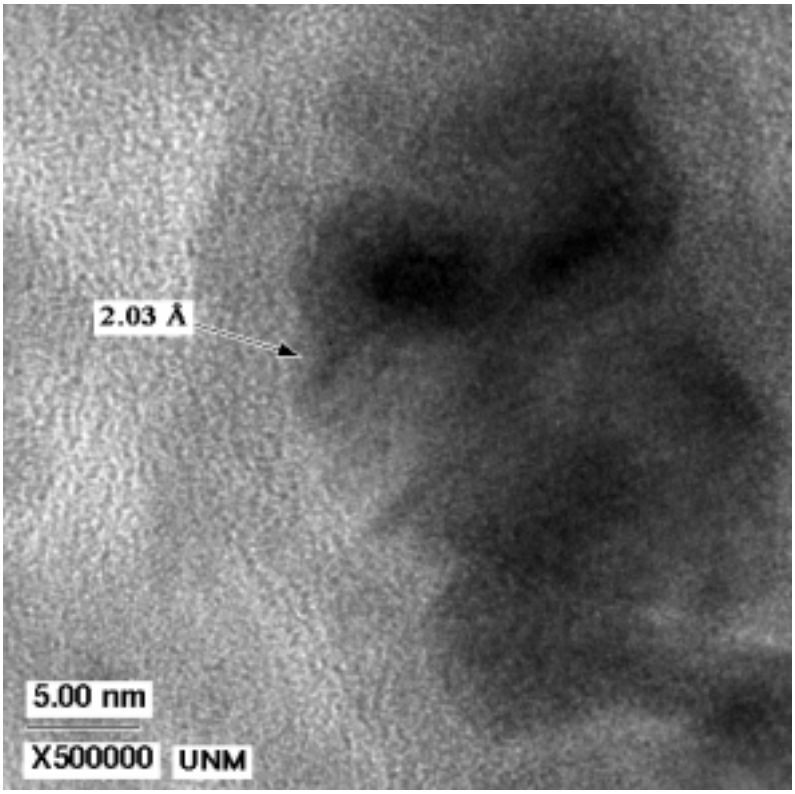


**Figure 3c**

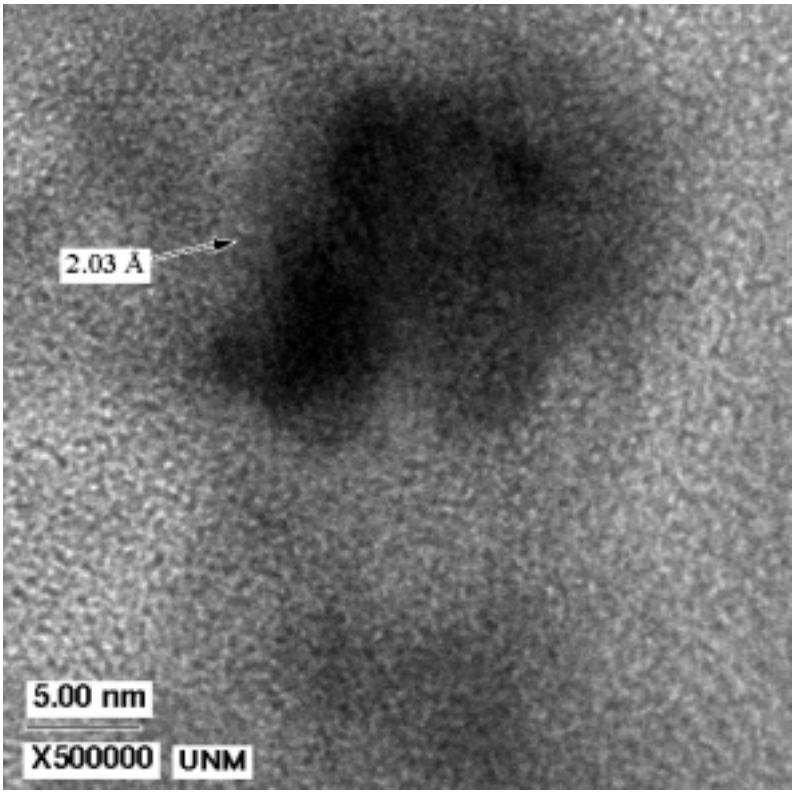


**Figure 3d**

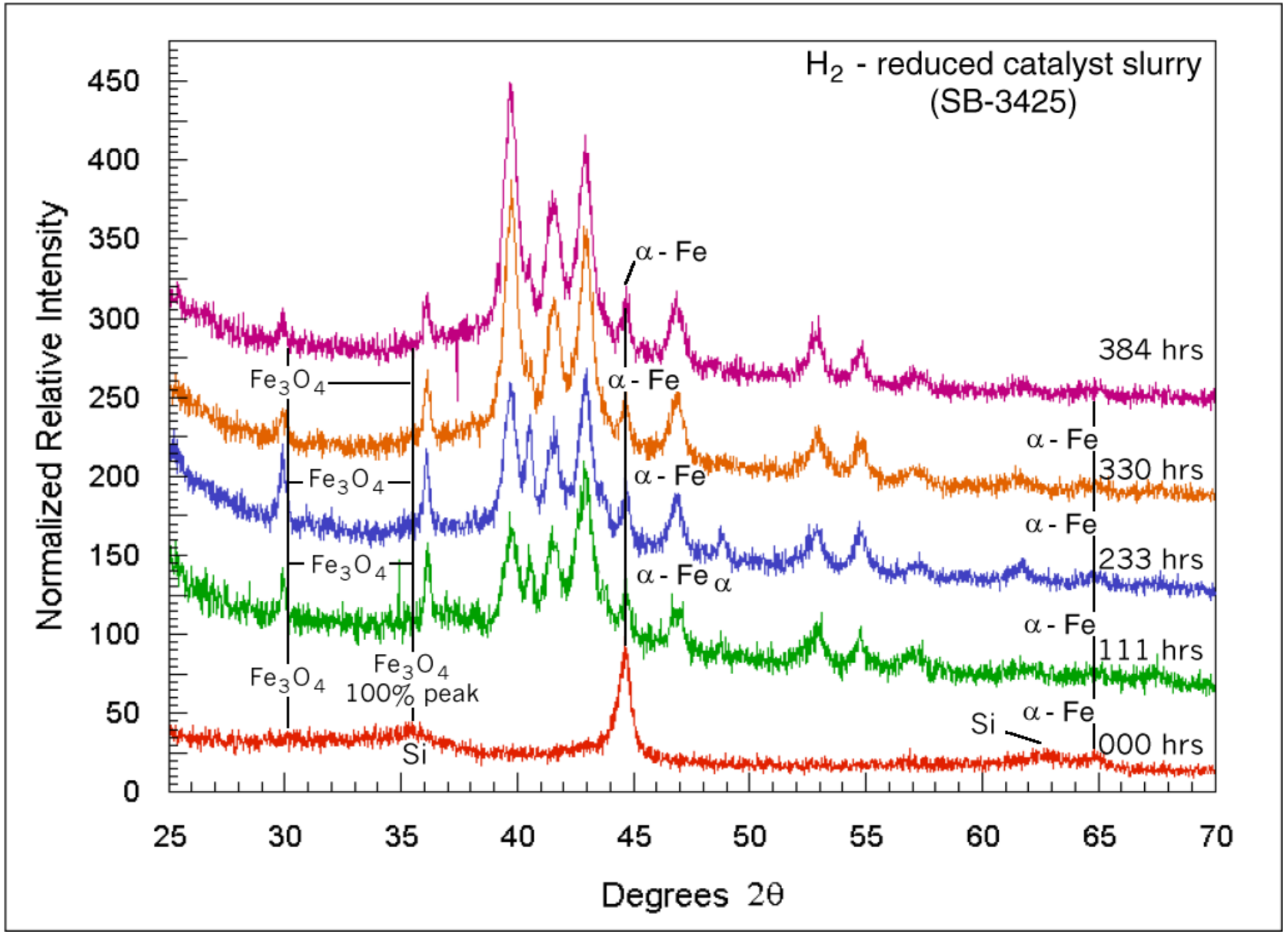
H2 - reduced catalyst slurry
(SB-3425)
Normalized Relative Intensity
Degrees 2θ
α - Fe
Fe3O4
Fe3O4
100% peak
Si
384 hrs
330 hrs
233 hrs
111 hrs
000 hrs

**Figure 4a**

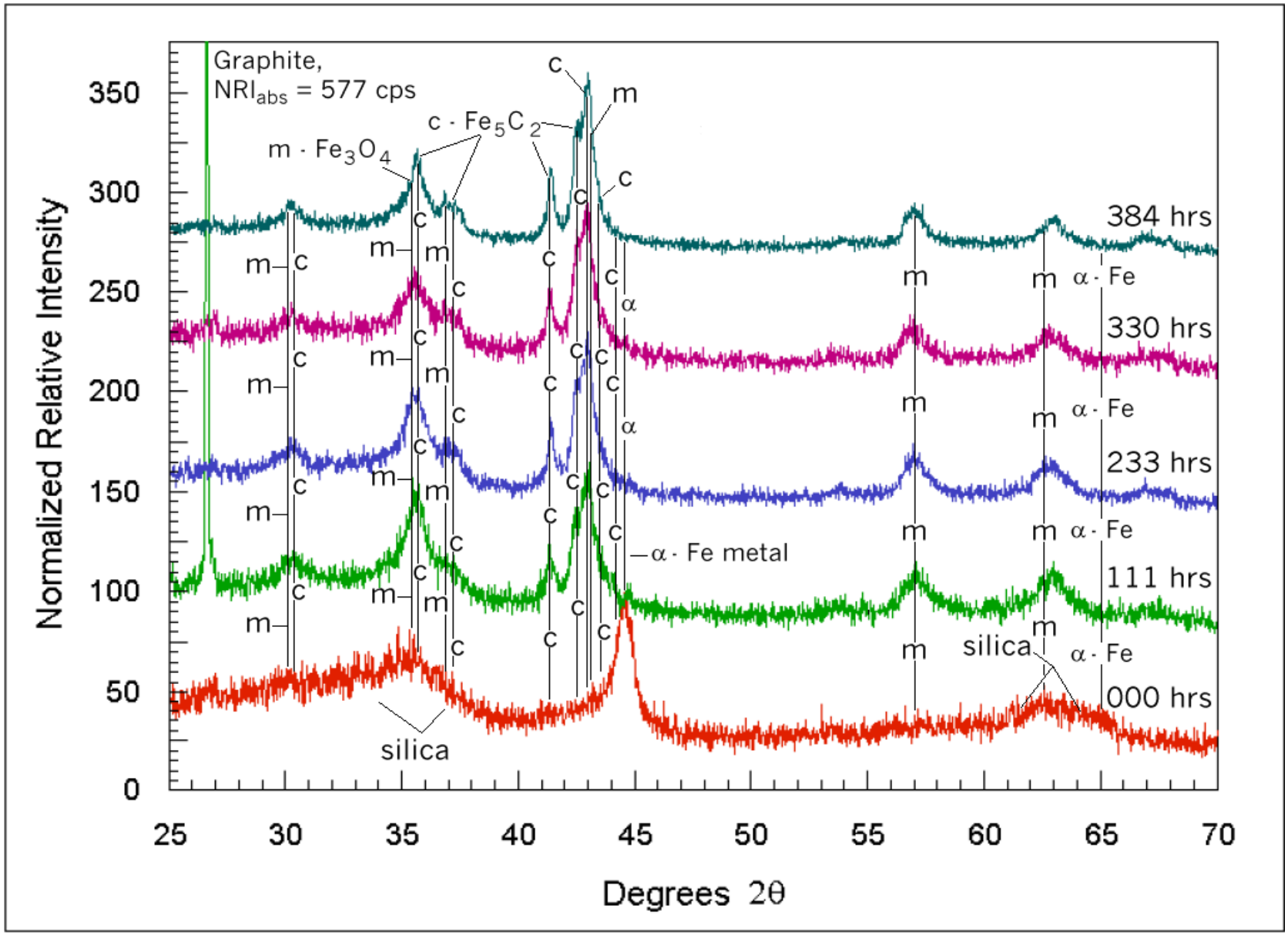
Graphite,
NRI$_{abs}$ = 577 cps
m · Fe$_3$O$_4$
c · Fe$_5$C$_2$
α · Fe metal
silica
384 hrs
330 hrs
233 hrs
111 hrs
000 hrs
α · Fe
Normalized Relative Intensity
Degrees 2θ
0
50
100
150
200
250
300
350
25
30
35
40
45
50
55
60
65
70

**Figure 4b**

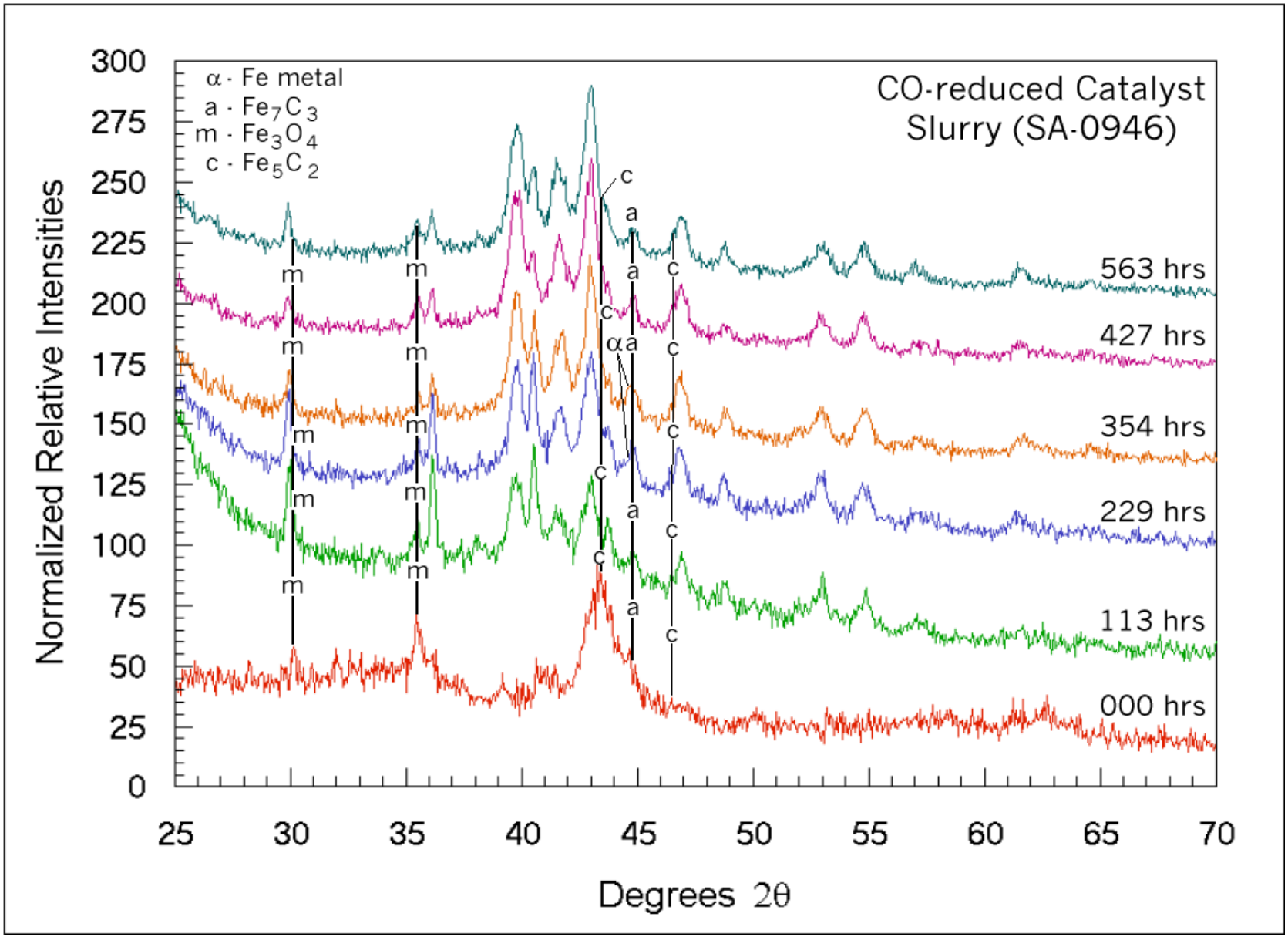
α - Fe metal
a - Fe7C3
m - Fe3O4
c - Fe5C2
CO-reduced Catalyst
Slurry (SA-0946)
563 hrs
427 hrs
354 hrs
229 hrs
113 hrs
000 hrs
Normalized Relative Intensities
Degrees 2θ
300
275
250
225
200
175
150
125
100
75
50
25
0
25
30
35
40
45
50
55
60
65
70

**Figure 4c**

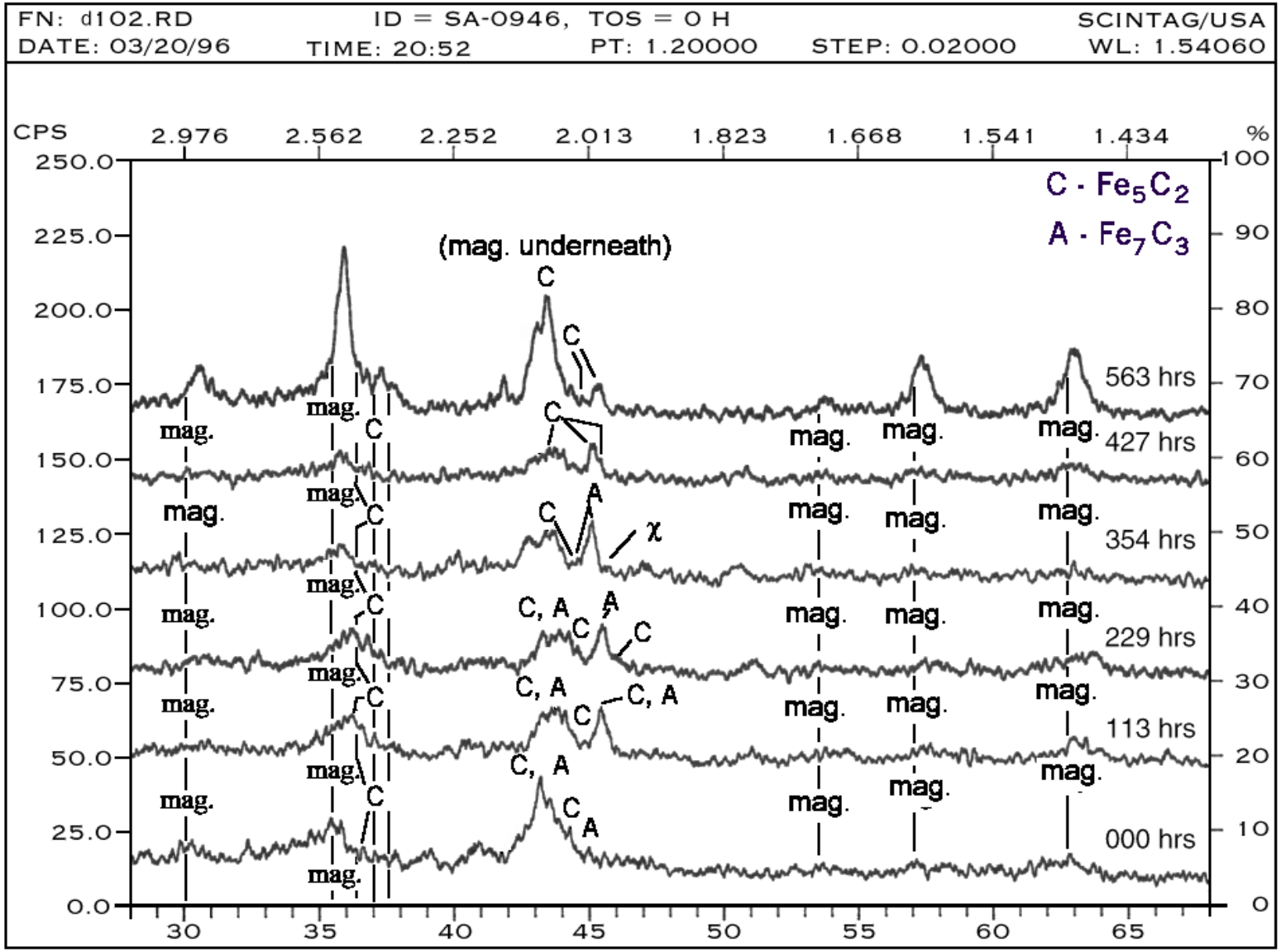
FN: d102.RD
ID = SA-0946, TOS = 0 H
SCINTAG/USA
DATE: 03/20/96
TIME: 20:52
PT: 1.20000
STEP: 0.02000
WL: 1.54060
CPS
2.976
2.562
2.252
2.013
1.823
1.668
1.541
1.434
%
C - Fe5C2
A - Fe7C3
(mag. underneath)
563 hrs
427 hrs
354 hrs
229 hrs
113 hrs
000 hrs
mag.
C
A
χ
250.0
225.0
200.0
175.0
150.0
125.0
100.0
75.0
50.0
25.0
0.0
100
90
80
70
60
50
40
30
20
10
0
30
35
40
45
50
55
60
65

**Figure 4d**

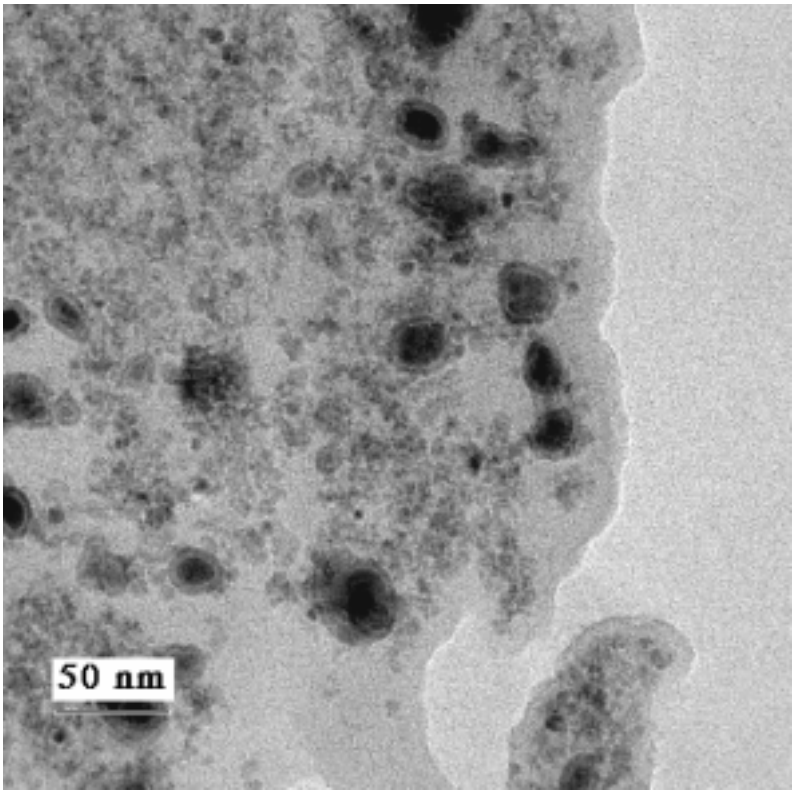


**Figure 5a**

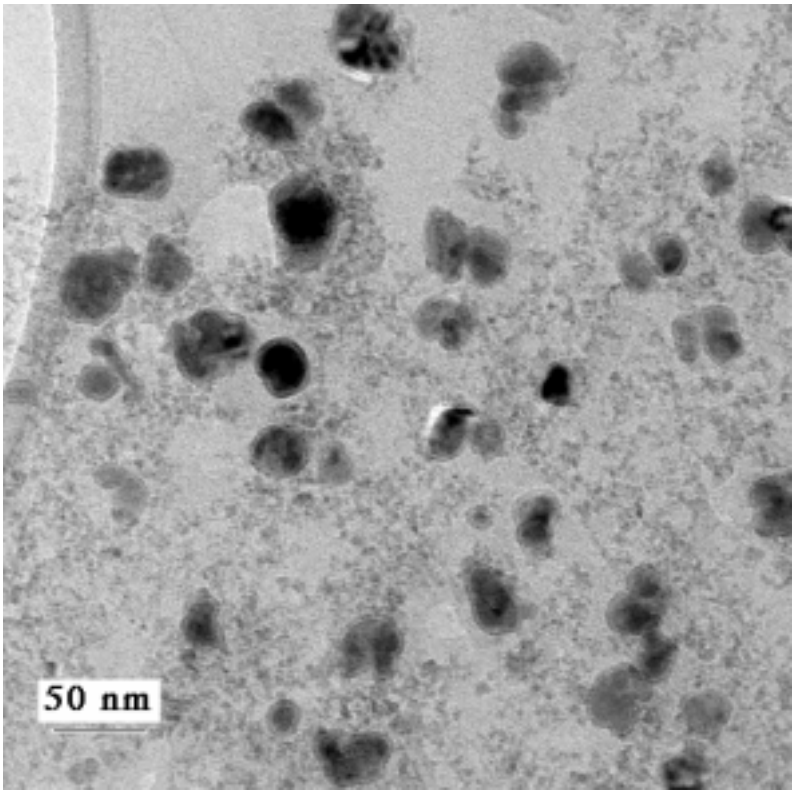


**Figure 5b**

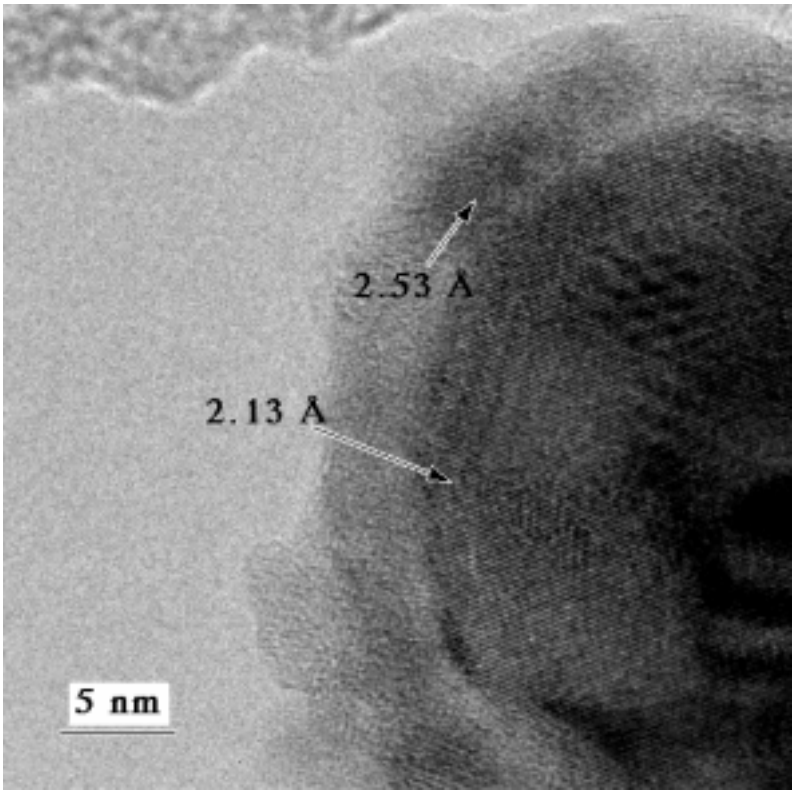


**Figure 5c**

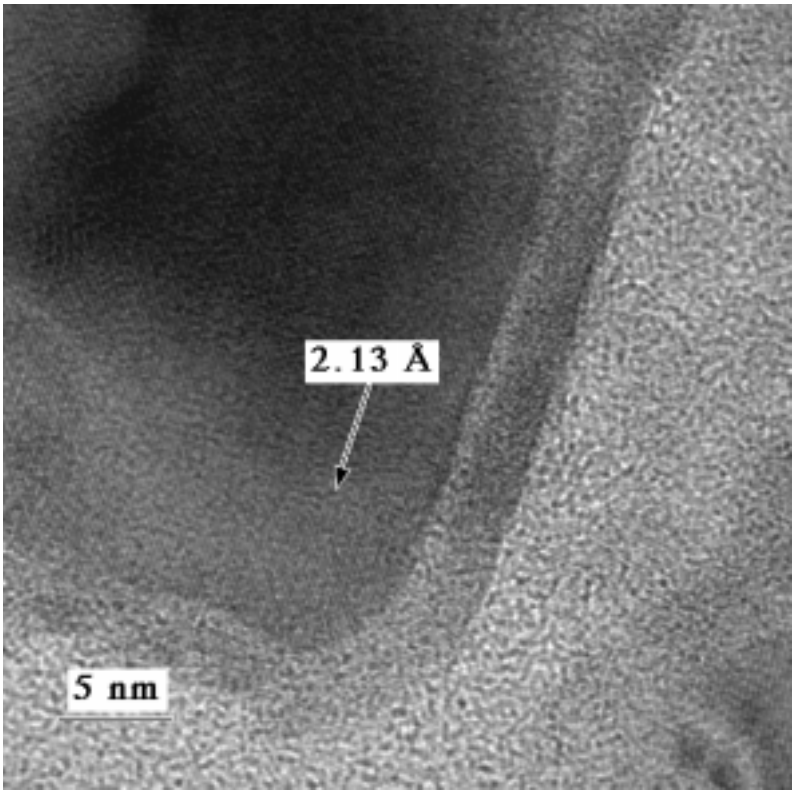


**Figure 5d**

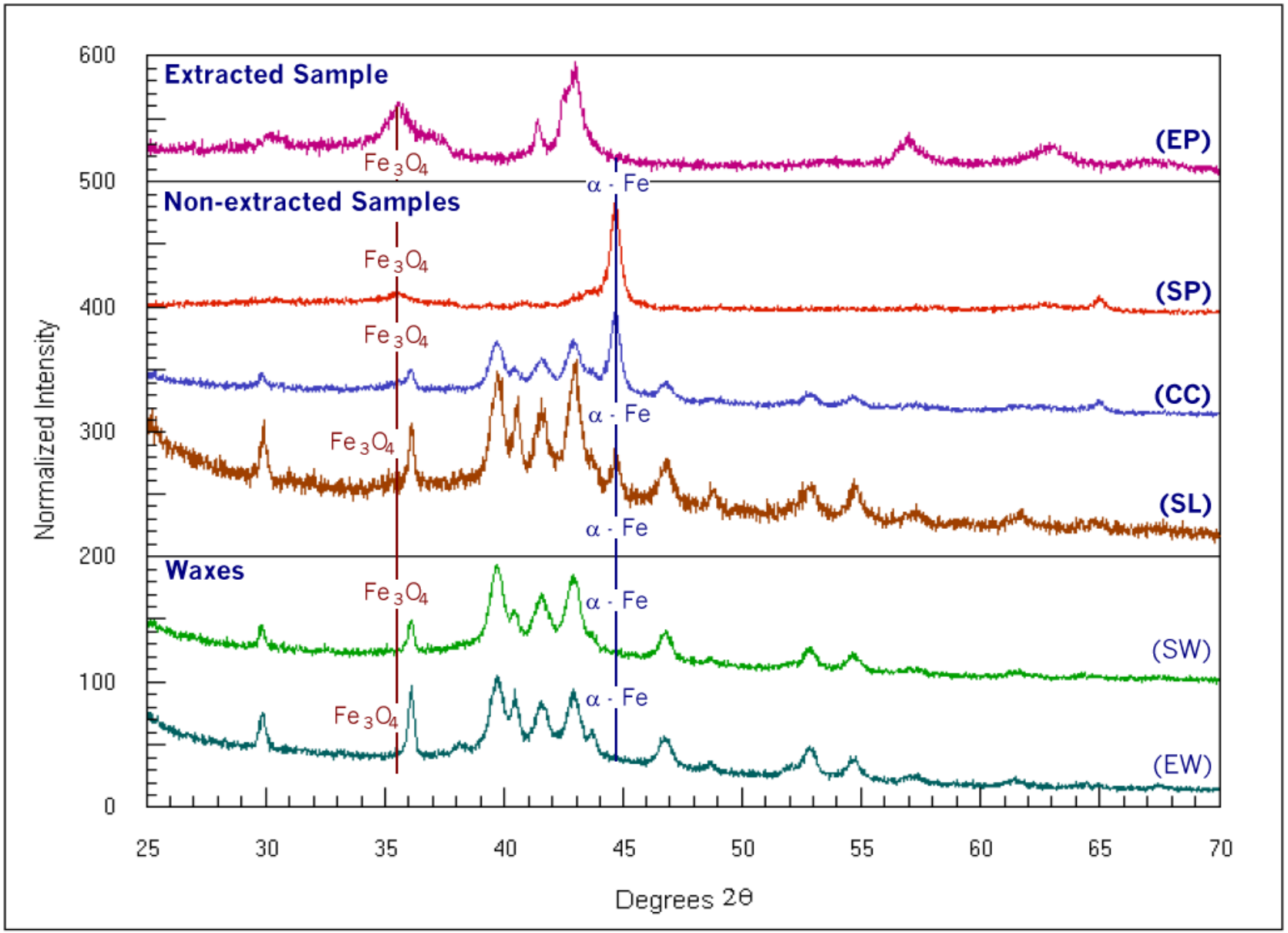
Extracted Sample
(EP)
Fe3O4
α - Fe
Non-extracted Samples
(SP)
(CC)
(SL)
Waxes
(SW)
(EW)
Normalized Intensity
Degrees 2θ
600
500
400
300
200
100
0
25
30
35
40
45
50
55
60
65
70

**Figure 6**

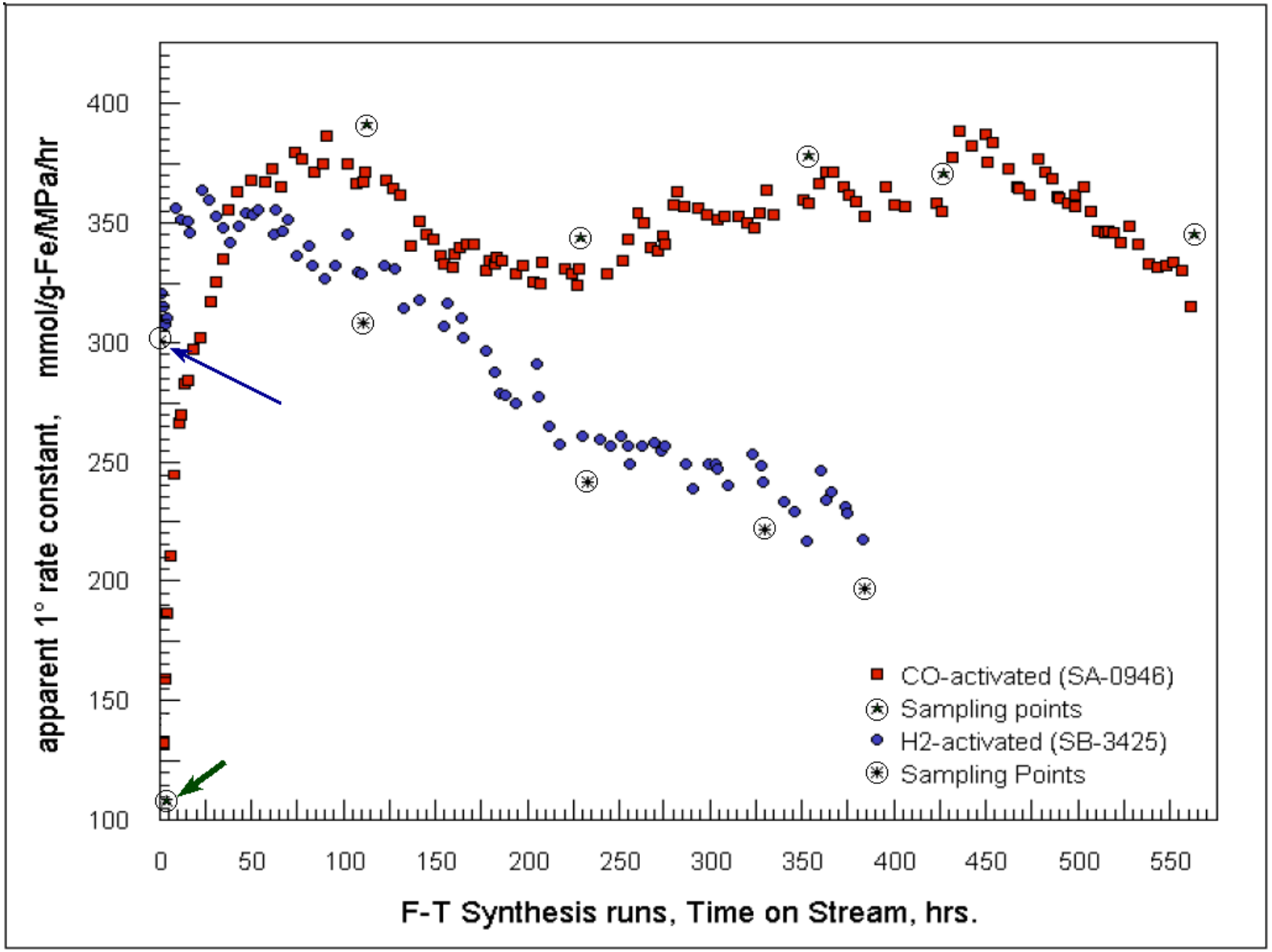
apparent 1° rate constant, mmol/g-Fe/MPa/hr
400
350
300
250
200
150
100
0
50
100
150
200
250
300
350
400
450
500
550
F-T Synthesis runs, Time on Stream, hrs.
CO-activated (SA-0946)
Sampling points
H2-activated (SB-3425)
Sampling Points

**Figure 7**